

<https://doi.org/10.1038/s43856-025-00942-3>

Protection against *APOE4*-associated phenotypes with the longevity-promoting intervention 17 α -estradiol in middle-aged male mice

Check for updates

Cassandra J. McGill¹, Amy Christensen¹, Wenjie Qian¹, Max A. Thorwald ¹, Jose Godoy Lugo¹, Sara Namvari¹, Olivia S. White¹, Caleb E. Finch ¹, Bérénice A. Benayoun ^{1,2,3,4,5} & Christian J. Pike ¹

Abstract

Background The apolipoprotein $\epsilon 4$ allele (*APOE4*) is associated with decreased longevity and increased vulnerability to age-related declines and disorders across multiple systems. Interventions that promote healthspan and lifespan represent a promising strategy to attenuate the development of *APOE4*-associated aging phenotypes. Here, we studied the ability of the longevity-promoting intervention 17 α -estradiol (17 α E2) to protect against impairments in *APOE4* versus the predominant *APOE3* genotype using early middle-aged mice with knock-in of human *APOE* alleles.

Methods Beginning at age 10 months, male *APOE3* or *APOE4* mice were treated for 20 weeks with 17 α E2 or vehicle then compared body-wide for indices of middle-aged phenotypes.

Results Across peripheral and neural measures, *APOE4* associates with poorer outcomes. Notably, 17 α E2 treatment generally improves outcomes in a genotype-dependent manner, favoring *APOE4* mice, including reductions in body weight, plasma leptin, hepatic steatosis, learning and memory, and oxidative damage in the brain. Plasma lipidomics and microglial transcriptomics show reductions in genotype-specific differences with 17 α E2 treatment.

Conclusions These findings demonstrate that *APOE4* promotes systemic and neural aging phenotypes linked to AD and that 17 α E2-mediated healthspan actions show a positive *APOE4* bias. Collectively, the findings suggest that longevity-promoting interventions may be useful in mitigating deleterious age-related risks associated with the *APOE4* genotype.

Age is a primary risk factor for systemic impairments, such as metabolic dysfunction and inflammation, as well as neural declines contributing to diminished cognitive abilities and increased risks of Alzheimer's disease (AD) and related disorders¹. In human populations, vulnerability to mortality and age-related dysfunction is modulated by genotype at the apolipoprotein E (*APOE*) locus, with generally detrimental effects associated with the $\epsilon 4$ genotype (*APOE4*). Compared to *APOE3*, the most common of

APOE alleles, *APOE2* is associated with increased longevity and decreased risk of cognitive impairment and AD^{2–4}. Conversely, *APOE4* is associated with reduced longevity^{2–4} and is the most significant genetic risk factor for both age-related cognitive impairment and AD pathogenesis^{3,5,6}. The primary roles of the apoE protein involve lipid trafficking and cholesterol homeostasis^{7–9} through which it impacts metabolism, inflammation, and several other systems^{3,5,10,11}. The apoE cascade hypothesis posits that *APOE*

Plain language summary

People with a particular sequence in a part of their DNA called *APOE* (named *APOE4*) are more likely to have a reduced lifespan and have a higher risk of developing some age-related disorders, including Alzheimer's disease. We tested whether a drug that extends lifespan and healthy aging in mice, called 17 α -estradiol (17 α E2), reduces the aging effects of *APOE4*. We compared male mice with different *APOE* sequences for 20 weeks during early middle age. As expected, we found that mice with the *APOE4* sequence showed more signs of aging, but that 17 α E2 improved several health-related measures, often with a bigger effect in mice with *APOE4*. These results suggest that treatments that promote healthy aging may be especially helpful for people with *APOE4*, potentially reducing their risk for age-related diseases such as Alzheimer's disease.

¹Leonard Davis School of Gerontology, University of Southern California, Los Angeles, CA, USA. ²Molecular and Computational Biology Department, USC Dornsife College of Letters, Arts and Sciences, Los Angeles, CA, USA. ³Cancer Biology Department, USC Keck School of Medicine, Los Angeles, CA, USA. ⁴USC Norris Comprehensive Cancer Center, Epigenetics and Gene Regulation, Los Angeles, CA, USA. ⁵USC Stem Cell Initiative, Los Angeles, CA, USA.

e-mail: bbenayou@usc.edu; cjpike@usc.edu

genotypes yield variations in apoE structure, lipidation, protein levels, receptor binding, and oligomerization that, in turn, result in diverse functional outcomes¹². In the context of *APOE4*, these variations are thought to drive body-wide homeostatic alterations that ultimately contribute to numerous age-related declines including vulnerability to cognitive decline and AD¹². Thus, the *APOE4* genotype may be linked to increased risks of dysfunction and disease by regulating aging processes.

Strategies to improve healthspan and lifespan have notable promise in reducing risks of age-related impairments across multiple body systems, perhaps especially in the context of *APOE4*. A variety of candidate longevity interventions have been tested through the NIA Interventions Testing Program (ITP). Given the relationship between *APOE4* and aging, we hypothesized that longevity interventions may prove efficacious against age-associated *APOE4* phenotypes. Out of the scores of compounds tested by the ITP, 17 α -estradiol (17 α E2) is one of the few that showed significant improvements in mean and maximum measures of male lifespan¹³, as well as improvements in various indices of systemic and brain aging^{14–22}. 17 α E2 is a naturally occurring diastereomer of the primary estrogen 17 β -estradiol but has comparatively weak estrogenic effects owing to reduced affinity for estrogen receptors²³. 17 α E2 has been shown to be protective in brain^{24–26} and peripheral tissues^{15,21,22,27}, in part by improving metabolism and reducing inflammation. The potential efficacy of 17 α E2 and other longevity-promoting interventions to attenuate *APOE4* phenotypes associated with deleterious aging outcomes is a promising strategy that has yet to be investigated.

Here, we evaluate the therapeutic potential of 17 α E2 to protect against the development of systemic and neural phenotypes associated with middle-age in *APOE3* versus *APOE4* genotypes. Specifically, we treated male mice with replacement of mouse *ApoE* with human *APOE3* or *APOE4* during the transition to middle age with 0 or 14ppm 17 α E2 for a 20-week period. As expected, the data show that age-related phenotypes are exaggerated with the *APOE4* genotype. Notably, our findings also demonstrate that while 17 α E2 treatment leads to improvements in both genotypes for some measures, it yields benefits in several systemic and brain outcomes only or greater in *APOE4* mice. To the best of our knowledge, this represents a new strategy to mitigate the progeroid effects of the *APOE4* genotype and provides proof-of-principle for a personalized medicine approach in a preclinical model.

Materials and methods

Animals and treatment

All male mice were homozygous for knock-in of human *APOE3* or *APOE4*. Only male mice were studied in this initial, proof-of-principle study as female mice are reported to exhibit comparatively limited healthspan and longevity benefits from 17 α E2^{13,27–31}. The mice were generated from a breeding colony of EFAD (*APOE*^{+/+}, 5x*FAD*^{+/+}) mice³², but were non-carriers of the 5x*FAD* Alzheimer's-related genes (*APOE*^{+/+}, 5x*FAD*^{-/-}). We genotyped a subset of the utilized mice for known alleles reported in the 5x*FAD* mouse strain, *Cdh23-ahl*, *Pde6b-rd1*, and *Trem2-S148E*, that could affect auditory, visual, and inflammatory measurement [See: <https://www.jax.org/strain/006554>], respectively. All animals tested ($n = 16$; 4 per experimental group) were homozygous for wild-type alleles. The colony was started from breeding pairs generously provided by Mary Jo LaDu (University of Illinois at Chicago). Mice were maintained in a vivarium under controlled temperature, a 12:12 light/dark schedule (lights on at 6:00 am), group housing when applicable, and *ad libitum* access to water and food (except when specified otherwise). Single-housed mice were supplemented with a twist chew. At 10–10.5 months of age, *APOE3* and *APOE4* mice were randomized (using covariate-adaptive randomization) to two dietary treatment groups ($n = 17–22$ /group): TestDiet 5LG6 chow [67.3% carbohydrate, 20.5% protein, 12.1% fat] formulated with 0 (Control diet) or 14.4 ppm 17 α E2 (Steraloids, Newport, RI) by TestDiet (Richmond, IN). This 17 α E2 dosage and delivery method were demonstrated to increase mean and maximum lifespan in male mice³³. Confounding factors were minimized through consistent location and timing of experiments. All

experiments took place between 8 am–12 pm. The experimental design is summarized in Fig. 1a.

The mice were kept on the diets over a treatment period of 20 weeks, during which body weight and food consumption were recorded weekly (Table 1). Body composition was measured at weeks 0 and 20 of treatment using a Bruker minispec whole body composition analyzer (Bruker LF90 Minispec, Bruker Optics, Billerica, MA). Mice were monitored daily for overall health, appearance, and euthanasia criteria, including >20% body weight decrease, lethargy, and poor grooming. After the 20-week experimental period, mice were euthanized through inhalation of carbon dioxide after overnight food withdrawal, followed by transcardial perfusion with 20 mL ice-cold 0.1 M PBS. The brains were rapidly removed, and one hemibrain was immersion-fixed for 48 hours in 4% paraformaldehyde/0.1 M PBS, then stored at 4 °C in 0.1 M PBS/0.03% NaN₃ until processing for immunohistochemistry. The other hemibrain was dissected into cortex, hippocampus, and hypothalamus. All portions were snap frozen for RNA or protein extraction. Plasma was collected and stored at –80 °C. Visceral and retroperitoneal fat pads and livers were dissected and weighed; all were snap frozen. Mice used for RNA-seq and lipidomics were not subjected to behavior, GTT, or fasting to avoid long-lasting effects of stress. This cohort was euthanized in the same manner as previously described. Whole blood was collected via cardiac puncture prior to perfusion for plasma isolation. One hemibrain was immediately used for microglia isolation. The other hemibrain was dissected into cortex, hippocampus, and hypothalamus. All procedures were conducted in accordance with the National Institutes of Health guidelines, under the supervision of veterinary staff, and following a protocol (#21269) approved by the University of Southern California Institutional Animal Care and Use Committee.

Glucose measurements

Mice were fasted for 16 hours overnight, and blood glucose levels were measured at week 0. At week 19, all mice (except for the RNA-seq cohort) were assessed using a glucose tolerance test (GTT) following 16 hours of fasting. In brief, baseline blood glucose was determined, then animals were orally gavaged with 20% D-glucose in water (2 g/kg). Blood glucose levels were measured through tail vein bleed and recorded 15, 30, 60, and 120 minutes after administration of the glucose using the Precision Xtra Blood Glucose and Ketone Monitoring System (9881465; Abbott Laboratories, Abbott Park, IL).

Behavioral assessments

Open field. A standard open field test was performed at week 15 on all mice (except for the RNA-seq cohort). The mice were moved to the behavior room 30 minutes prior to testing to acclimate. Mice were then placed into an open field box (40 cm x 40 cm) and allowed to explore freely for 10 min. The following behaviors were recorded: velocity (cm/s); travel distance (cm); ambulatory time (s).

Spontaneous alternation test. At 15 weeks, animals were tested for spontaneous alternation behavior in the Y maze, a hippocampus-dependent task that assesses attention to novelty and spatial memory^{34,35}. Mice were brought to the behavior room to acclimate 30 minutes prior to testing. The Y maze consists of 3 arms 40 cm long and 7 cm wide. Each mouse was placed in one arm and allowed to explore the arena for 5 minutes. Arm entries were recorded if the mouse placed 2 paws into the arm. Three consecutive, nonrepeating entries were considered a correct alternation.

Barnes maze. The Barnes maze test was performed at week 16 using a modified Barnes maze protocol³⁶. The maze consisted of an open circular platform (91.5 cm in diameter) with 20 evenly spaced holes (5 cm in diameter) located along the border, with a rectangular escape box (11 cm L x 5 cm W x 5 cm H) located beneath one hole. Using spatial-visual clues on each side of the platform, mice were trained to find the escape box. On each day of testing, mice were taken into the behavior

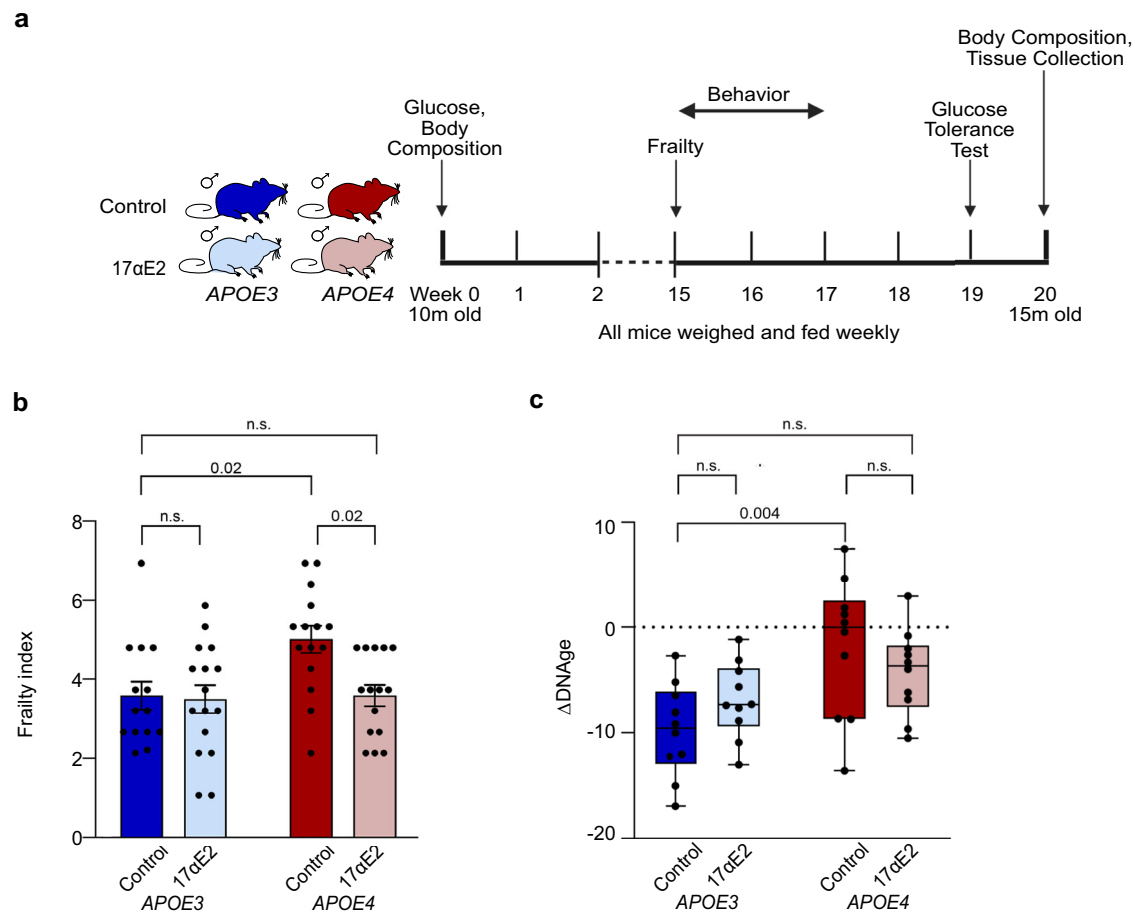


Fig. 1 | APOE4 genotype increases aging phenotypes that are ameliorated by 17α-estradiol. a Schematic overview of experimental design. Male APOE3 and APOE4 targeted-replacement mice were fed with normal chow or chow supplemented with 14.4 ppm 17α-estradiol (17αE2) for 20 weeks beginning at age 10 to 10.5-month-old. At 15 weeks of treatment, animals were assessed for frailty and behavioral changes. At 19 weeks of treatment, a glucose tolerance test was performed. Tissues were collected at 20 weeks following treatment initiation. **b** Measure of systemic aging

using a phenotypic 26-point frailty index ($n = 14$ mice/APOE3 Control, 16/APOE3 17αE2, 15/APOE4 Control, 15/APOE4 17αE2). **c** Measure of biological aging using a DNA methylation clock derived from liver tissue ($n = 10$ mice/all groups). In **b** and **c**, dark blue indicates APOE3 control, light blue indicates APOE3 17αE2, dark red indicates APOE4 control, and light red indicates APOE4 17αE2. Data show mean \pm SEM. P-values denote statistical significance in a 2-way ANOVA with a Tukey *post-hoc* test.

Table 1 | 17α-Estradiol decreases body weight, food intake, and fat mass while increasing lean mass more strongly in male APOE4 mice. All data show mean \pm standard deviation

Measure	APOE3 Control	APOE3 17αE2	APOE4 Control	APOE4 17αE2
Body Mass % change from Week 0	2.18 \pm 1.65	-6.22 \pm 0.79 (-7.16 \pm 2.52) $p = 0.035$	-2.92 \pm 1.69	-17.22 \pm 1.75 (-15.09 \pm 2.52) $p < 0.0001$
Food Intake kcal	14.13 \pm 0.63	13.54 \pm 0.46 (-4.10 \pm 3.93)	14.37 \pm 0.39	12.82 \pm 0.72 (-10.82 \pm 4.52) $p < 0.0001$
Week 20 Lean Mass % of Body Mass	59.67 \pm 6.50	65.97 \pm 2.95 (+5.02)	53.00 \pm 4.37	62.36 \pm 4.88 (+8.12) $p = 0.0001$
Week 20 Fat Mass % of Body Mass	27.67 \pm 9.36	20.19 \pm 4.26 (-15.62)	36.94 \pm 7.11	25.87 \pm 6.39 (-17.63) $p = 0.0001$

(Number in parentheses indicates % change relative to genotype-matched control).

room 30 minutes prior to testing to allow them to acclimate. On the first day of the Barnes maze, the escape box was removed, and mice were habituated to the maze. Each mouse was given a single habituation trial in which they were placed in an opaque cylinder in the center of the maze. After 10 seconds had elapsed, the cylinder was removed, allowing the mice to explore the maze freely for 3 minutes under red light. On the second day of the Barnes maze, mice were placed in a cylinder in the

center of the maze, a bright light and buzzer were turned on, and after 10 seconds had elapsed, the cylinder was removed. Mice were gently guided into the escape box, after which the light and buzzer were turned off. Mice stayed in the escape box for 1 minute before they were returned to their home cages. After this initial training session, each testing day (including the initial training session day) consisted of 3 training trials per day with an intertrial interval of 15 minutes. Between trials, mice were

kept in their own home cages, and the maze was cleaned with 70% ethanol. Acquisition training continued for 3 more days (4 training days total). During each trial, mice were placed in a cylinder in the center of the maze, a light and buzzer were activated, and after 10 seconds the cylinder was removed. Mice were given 3 minutes to explore freely and locate the escape box. The trial ended either when 3 minutes elapsed or when mice found and entered the escape box. Once a mouse found and entered the escape box the light and buzzer were turned off, and the mouse stayed inside the box for 1 minute. If the mouse did not find the escape box after 3 minutes of exploration, they were gently guided into the escape box and stayed inside the box for 1 minute. To ensure that the hidden escape box was not visible to the mice, three decoy boxes (5 cm L x 5 cm W x 2.5 cm H) were placed throughout the maze. 48 hours after the last acquisition trial, mice were given a probe trial in which the escape box was removed. On the probe trial day, mice were placed in the cylinder in the center of the maze, and a light and buzzer were turned on. After 10 seconds the cylinder was removed, and mice were given 3 minutes to explore freely. All tests were recorded using Noldus Ethovision XT software version 14.

Novel object placement and recognition. Novel object placement (NOP) and recognition (NOR) were performed at week 17 of treatment using a modification of a previously described protocol³⁷. After the Barnes maze probe trial, one small plastic Lego block was placed in each home cage to habituate the mice to the objects. On each day of testing, mice were taken into the behavior room to habituate for 30 minutes prior to testing. Forty-eight hours after the introduction of the block, mice were placed in the empty arena (40 cm x 40 cm), facing the wall that was nearest to the experimenter, and explored for 5 minutes to habituate to the arena. Twenty-four hours after the first habituation, the second habituation was performed in the same way. Twenty-four hours after the second habituation session, mice were placed in the empty arena and explored for 2 minutes, followed by returning to their home cages. The sampling trial consisted of two identical objects placed in the northeast and northwest corners of the arena, and mice were placed in the arena with their heads positioned opposite to the objects. They explored both objects until they accumulated a total of 30 seconds of exploration time, with a maximum of 20 minutes allowed for completion of training. Four hours after sampling, mice were placed in the testing arena in which one of the identical objects was moved to the southeast or southwest corner. The location of the moved object was counter-balanced across all mice. Mice were allowed to explore both objects until they accumulated a total of 30 seconds of exploration time, with a maximum of 20 minutes allowed for completion. Twenty-four hours after sampling, mice were placed in the testing arena in which a novel object was substituted for one of the familiar objects. They explored both objects until they accumulated a total of 30 seconds of exploration time, with a maximum of 20 minutes allowed for completion. Data are presented as a discrimination index, which is defined as the time spent with the novel object minus the time spent with the familiar object divided by the total exploration time. All tests were recorded using Noldus Ethovision XT software version 14.

Frailty measurement

The frailty index (FI) score was calculated for each mouse using a 26-point frailty index, which was modified from a 31-item frailty index³⁸ to omit measures of vestibular disturbance, hearing loss, and vision loss due to the subjective nature of the scoring to ensure consistency across investigators. Other measures excluded from FI assessment include body weight and body composition due to baseline differences that are measured separately. All frailty measures are reported in Supplementary Data S1A. Body temperature was recorded three times (Supplementary Data S1B), and the average was used for scoring (Supplementary Data S1A). FI assessment included evaluation of the integument, the physical/musculoskeletal system, the ocular/nasal system, the digestive/urogenital system, the respiratory system, body temperature, and signs of discomfort. The severity of each deficit was rated with a simple scale: 0, 0.5, and 1. A score of 0 was given if there were no

signs of a deficit, a score of 0.5 was given to a mild deficit, and a score of 1 indicates a severe deficit. All these values were summed up, giving a frailty score between 0 and 26 for each mouse. The researcher performing the measurement was blinded to all groups.

Plasma leptin quantification

Whole blood was collected via cardiac puncture and placed into a plasma collection tube containing EDTA (367856; BD Biosciences, Franklin Lakes, NJ). Plasma leptin was determined using an ELISA kit (EZML-82K; Millipore Sigma, St. Louis, MO) according to the manufacturer's instructions.

Liver Oil Red O (ORO) staining and quantification

Frozen livers were sectioned at 10 μ m using a cryostat at -13°C . 4 pieces were collected on the same glass slide for each animal ($N = 8/\text{group}$). The slides were stored in the -20°C freezer until ORO staining. Frozen liver sections were brought to room temperature, dipped 10 times into freshly prepared 60% triethyl phosphate, then stained with a solution of 0.5% Oil Red O/60% triethyl phosphate for 16 minutes. Sections were rinsed in a gentle stream of running water for 2 minutes and put into clean water before mounting with prewarmed glycerin jelly. Stained sections were stored at room temperature for one day, after which high magnification brightfield images (four sections/liver, one field/section, 20X objective) were collected by unbiased sampling for a total of 4 images per liver. Images were captured using an Olympus BX50 microscope and DP74 camera paired with a computer running CellSens software v1.11 (Olympus). Images were converted to grayscale and thresholded using NIH ImageJ 1.50i to yield binary images separating positive and negative immunostaining. The Analyze-Measure tool was used to obtain the value of the percentage of the ORO-positive area.

DNA methylation sequencing and epigenetic age calculation

Frozen liver tissue ($n = 10/\text{group}$) was processed by the Zymo Research DNAge Service (Tustin, CA). Briefly, DNA was purified from the frozen liver using the Quick-DNA Miniprep Plus kit (D4068, Zymo Research, Tustin, CA). After quality and quantity checks, bisulfite conversion was performed using the EZ DNA Methylation-Lightening kit (D5030, Zymo Research, Tustin, CA). Samples were enriched for >500 age-associated gene loci and sequenced on an Illumina NovaSeq6000 instrument. Sequenced reads identified by Illumina's base calling software were aligned to the mouse reference genome using Bismark. Cytosine methylation level was determined as the number of reads reporting a C, divided by the total number of reads reporting a C or T. DNA methylation values were used to assess DNAge according to Zymo's proprietary DNAge predictor.

Lipidomics

Lipidomics was performed by the UCLA Lipidomics Core. For homogenized tissue, 50–100 mg of tissue was collected in a 2 mL homogenizer tube pre-loaded with 2.8 mm ceramic beads (19-628; Omni, Kennesaw, GA). 0.75 mL PBS was added to the tube and homogenized in the Omni Bead Ruptor Elite (3 cycles of 10 seconds at 5 m/s with a 10 second dwell time). Homogenate containing 2–6 mg of original tissue was transferred to a glass tube for extraction. A modified Bligh and Dyer extraction³⁹ was carried out on all samples. Prior to biphasic extraction, an internal standard mixture consisting of 70 lipid standards across 17 subclasses was added to each sample (AB Sciex 5040156, Avanti 330827, Avanti 330830, Avanti 330828, Avanti 791642). Following two successive extractions, pooled organic layers were dried down in a Thermo SpeedVac SPD300DDA using ramp setting 4 at 35°C for 45 minutes with a total run time of 90 minutes. Lipid samples were resuspended in 1:1 methanol/dichloromethane with 10 mM Ammonium Acetate and transferred to robovials (Thermo 10800107) for analysis.

Samples were analyzed on the Sciex 5500 with DMS device (Lipidizer Platform) with an expanded targeted acquisition list consisting of 1450 lipid species across 17 subclasses at the UCLA Lipidomics Core. Differential Mobility Device on Lipidizer was tuned with EquiSPLASH LIPIDOMIX (Avanti 330731). Data analysis performed on an in-house data analysis

platform comparable to the Lipidizer Workflow Manager⁴⁰. Instrument method including settings, tuning protocol, and MRM list available in Ref. 40. Quantitative values were normalized to mg of tissue.

Lipidomics bioinformatics analysis

Lipids not detected across all samples were discarded. A total of 841 lipids were originally detected across plasma and cortex; after filtering, 565 remained for plasma and 501 for cortex. The dataset was first normalized to the amount of tissue or plasma. Then, variance stabilizing normalization was applied to the data using 'limma' v.3.48.3, as recommended by previous studies^{41,42}. Differential analysis was performed using 'limma' in R, and lipids with an FDR < 5% were considered statistically significant. Lipid ontology enrichment analysis was performed using the LION web-based ontology enrichment tool, with all detected lipids used as the background⁴³. Plasma lipidomics and enrichment analyses can be found in Supplementary Data 2A–D.

Microglia isolation from fresh mouse brain

Following dissection, one hemisphere from a dedicated cohort that included all experimental groups ($n = 4\text{--}5/\text{group}$) was used to isolate microglia for RNA sequencing. This hemisphere was temporarily stored in 5 mL of HBSS buffer (w/o Ca^{2+} , Mg^{2+}) (88284, Thermo Fisher Scientific, Waltham, MA). Tissue dissociation was performed using the Worthington Papain Dissociation System (LK003150; Worthington Biochemical, Lakewood, NJ) according to the manufacturer's instructions. The dissociated cell pellet was resuspended in 1 mL of MACS buffer (130-091-221; Miltenyi Biotec, Bergisch Gladbach, North Rhine-Westphalia, Germany). Microglia were isolated using Miltenyi CD11b Microglia Microbeads (130-093-636; Miltenyi Biotec, Bergisch Gladbach, North Rhine-Westphalia, Germany) according to the manufacturer's instructions. Cell number and viability were determined using trypan blue exclusion on an automated COUNTESS cell counter (Thermo Fisher Scientific, Waltham, MA). Purified cells were pelleted at 300 $\times g$ then snap-frozen in liquid nitrogen until RNA extraction.

RNA isolation and RNA-seq library preparation

For RNA isolation, frozen cell pellets were resuspended in 1 mL of Trizol reagent (15596018; Invitrogen, Carlsbad, CA) and total RNA was purified following the manufacturer's instructions. RNA quality was assessed using the Agilent Bioanalyzer platform at the USC Genome Core using the RNA integrity number. Then, 500 ng of total RNA was subjected to ribosomal-RNA depletion using the NEBNext rRNA Depletion kit (E7850L; New England Biolabs, Ipswich, MA), according to the manufacturer's protocol. Strand-specific RNA-seq libraries were then constructed using the SMARTer Stranded RNA-seq kit (634485; Clontech, Kusatsu, Shiga, Japan), according to the manufacturer's protocol. Libraries were quality controlled on the Agilent Bioanalyzer 2100 platform at the USC Genome Core before multiplexing the libraries for sequencing. Paired-end 150-bp reads were generated on the Illumina NovaSeq6000 platform at the Novogene Corporation (Sacramento, CA). Raw sequencing reads have been deposited to the Sequence Read Archive under accession PRJNA1078754.

RNA-seq bioinformatic analysis pipeline

Paired-end 150-bp reads were hard-trimmed to 75 bp using Trimmomatic v0.39⁴⁴. Trimmed reads were mapped to the mm39 genome reference using STAR v.2.7.0e⁴⁵. Read counts were assigned to genes from the UCSC mm39 reference using subread v.2.0.2⁴⁶ and were imported into R version 1.4.1717 to perform differential gene expression analysis.

Only genes with mapped reads in at least half of the RNA-seq libraries were considered to be expressed and retained for downstream analysis. We used surrogate variable analysis (SVA) to estimate and correct for unwanted experimental noise⁴⁷. R package 'sva' v.3.40 was used to estimate surrogate variables, and the `removeBatchEffect` function from 'limma' v.3.48.3 was used to regress out the effects of surrogate variables and RNA integrity differences (RNA integrity number scores) from raw read counts. The 'DESeq2' R package (DESeq2 v.1.32.0) was used for further processing of the

RNA-seq data in R⁴⁸. Genes with FDR < 5% were considered statistically significant and are reported in Supplementary Data 3A–D. We found a non-linear relationship of between treatment the genotypes and thus modeled treatment and genotype separately. Given the superiority of modern RNA-seq methodology, RT-qPCR confirmation of results is not required^{49–52}. The following comparisons were performed: *APOE3* control to *APOE4* control, *APOE3* control to *APOE3* 17aE2, *APOE4* control to *APOE4* 17aE2, and *APOE3* control to *APOE4* 17aE2.

Dimensionality reduction

To perform multi-dimensional scaling (MDS) analysis⁵³, we used a distance metric between samples based on Spearman's rank correlation value (1-Rho), which was then provided to the core R command 'cmdscale'. Dimensionality reduction was applied to DESeq2 VST-normalized counts.

Functional enrichment analysis

The Gene Set Enrichment Analysis (GSEA) paradigm, through its implementation in the R package 'ClusterProfiler' v4.0.5⁵⁴, and Bioconductor annotation package 'org.Mm.eg.db' v3.13.0 were used to perform the functional enrichment analysis. The DESeq2 t-statistic was used to generate the ranked list of genes for functional enrichment analysis, for both genotype and treatment effects. The top 5 up- and down-regulated Gene Ontology (GO) terms per genotype are shown in figures if at least that many passed the FDR < 5% significance threshold (Fig. 5G, H). All significant GO terms are reported in Supplementary Data 3E–H.

Immunohistochemistry

Hemibrains fixed in 4% paraformaldehyde (A11313, Alfa Aesar, Ward Hill, MA) for 48 hours were transferred into 20% sucrose in PBS overnight at 4 °C until they sank to the bottom of the tube. Brains were then coronally sectioned at 20 μm using a cryostat (Leica Biosystems, Deer Park, IL). Four sections per well were stored in 0.03% sodium azide in PBS at 4 °C until immunohistochemistry was performed. Every eighth section from approximately -0.95 mm to -2.90 mm was immunostained with ionized calcium binding adaptor molecule 1 (Iba-1; 1:2000; 019-19741; FUJIFILM Wako, Richmond, VA) or glial fibrillar acidic protein (GFAP; 1:1000; G3893-100uL; Dako, Santa Clara, CA). For Iba1 staining, brain sections were first incubated with 10 nM EDTA (pH = 6) at 95 °C for 10 minutes. No antigen retrieval pretreatment was performed for GFAP staining. For both Iba1 and GFAP staining, sections were rinsed with 0.1 M Tris-buffered saline (TBS) and treated with an endogenous peroxidase blocking solution (3% H_2O_2 , 10% methanol in TBS) for 10 minutes. Sections were rinsed in 0.2% Triton-X in TBS before being blocked for 30 minutes in blocking solution. For Iba1, the blocking solution contained 2% bovine serum albumin (BSA) in TBS. For GFAP, the blocking solution contained 2% BSA and 2% normal goat serum in TBS. Sections were incubated with primary antibodies in their respective blocking solutions overnight at 4 °C. The next day, sections were rinsed in 0.1% Triton-X in TBS and incubated for 1 hour in their respective biotinylated secondary antibody diluted in blocking solution. Sections were rinsed once more in 0.1% Triton-X in TBS, then incubated in an avidin-biotin complex (PK-6100; Vectastain ABC Elite kit, Vector Laboratories, Newark, CA) for 1 hour. To visualize immunoreactivity, sections were incubated for 5 minutes using diaminobenzidine tetrahydrochloride (SK-4100; Vector Laboratories, Newark, CA).

To quantify Iba1 and GFAP immunoreactivity, non-overlapping high magnification brightfield images were collected from the CA1 hippocampal subfield (three fields/section, 20 \times objective) across four tissue sections per brain, for a total of ~ 12 images per brain. Images were captured using an Olympus BX50 microscope and DP74 camera paired with a computer running CellSens software v1.11 (Olympus). Images were converted to grayscale and thresholded using NIH ImageJ 1.50i to yield binary images separating positive and negative immunostaining. Iba1 and GFAP load was calculated as the percentage of total pixels that were positively immunolabeled.

Brain tissue extractions

Brain cerebral cortices were homogenized with a motorized pestle in RIPA buffer without SDS (30 mg tissue: 150 μ L) with protease (P2714, Millipore, Bedford, MA, USA) and phosphatase (78427, Thermo Fisher Scientific, Waltham, MA) inhibitors⁵⁵. Homogenates were centrifuged at 10,000 \times g for 1 hour at 4 °C, and supernatant was recovered for evaluation of soluble amyloid- β peptides. Proteins were quantified using Pierce's 660 nm assay (22660, Thermo Fisher Scientific, Waltham, MA). Lipid rafts were isolated by kit using 35 mg of cerebral cortex (LR-039, Invent Biotechnologies, Plymouth, MN). Lipid rafts were previously validated against traditional ultracentrifugation methods⁵⁵.

Dot blots

Twenty-five μ g of RIPA or 5 μ g of lipid raft protein lysate was loaded onto a dot blot apparatus (Bio-Rad, Hercules, CA, USA) and filtered through 0.45 μ m PVDF for 2 hours by gravity filtration. Membranes were stained with Revert 700 (926-11011, LICOR, Lincoln, NE, USA), imaged, and blocked for 1 hour with Intercept blocking buffer (927-70001, LICOR) before incubation for 16 hours with primary antibodies for A β 40, (1:500 dilution, Biologend, San Diego, CA, USA), and HNE (1:1000 dilution, ABN249, Millipore, Bedford, MA, USA). Membranes were visualized on a LICOR 9120 using fluorescent-conjugated secondary antibodies. Images were analyzed by ImageJ and corrected for total protein load.

Statistics and reproducibility

All data are reported as the mean \pm the standard error of the mean. The source data for Figs. 1–3, and 6 and Supplementary Figs. 1, 2, 5 and 6 are in Supplementary Data 4. Data were analyzed using GraphPad Prism version 5 (biochemical, behavioral, and metabolic data) or R version 1.4.1717 ('omic' data). All data were checked for normal distribution using the Shapiro-Wilk test. If a dataset was found not normally distributed, Mann-Whitney tests were used. Non-normally distributed datasets include oil red O staining, spontaneous alternation behavior, novel object placement, Iba1 immunohistochemistry, and open field: time in center. For normally distributed data, which described most of the group comparisons, two-way or three-way ANOVAs followed by Tukey *post-hoc* were performed. Two-way repeated-measure analysis of variance, followed by Tukey *post-hoc* tests, was run for all data measured over time. The Grubbs' outlier test was performed whenever possible outliers were observed; no significant outliers were found. Comparisons with $p < 0.05$ were considered statistically significant. All statistics are listed in Supplementary Data 5.

Animals were given a generic study number to allow for blinding to experimenters after initial allocation; experimenters were unblinded after data were analyzed (e.g., processing images, scoring behavior videos) to run statistical tests. We selected the sample size based on previously published literature conducting similar experiments, ensuring we used the minimal number of mice required to achieve statistical significance while maintaining the integrity of our analyses. Animals were excluded if they did not complete the study. Four control *APOE3*, one 17 α E2 *APOE3*, two control *APOE4*, and no 17 α E2 *APOE4* animals died prematurely. Studies performed in vivo include multiple cohorts to ensure replication of results. Additionally, biological replicates (individual animals) are included in all -omics measures.

Results

17 α E2 improves frailty phenotypes in male *APOE4* mice

Even in the absence of AD pathology, *APOE4* associates with both premature aging phenotypes and decreased lifespan in humans and mice⁴. To determine if the longevity-promoting intervention 17 α E2 provides greater protection against systemic phenotypes associated with middle-age in the context of the *APOE4* allele, we use strains of mice with humanized *APOE3* or *APOE4* sequences³². Since the NIA Intervention Testing Program (ITP) showed anti-aging effects of 17 α E2 only in males¹⁵, we decided to focus specifically on male mice in the study. Thus, we fed *APOE3* or *APOE4* knock-in male mice with normal chow or chow supplemented with

14.4 ppm 17 α E2, the dose shown to have anti-aging effects³¹, for a period of 20 weeks starting at 10 months of age (Fig. 1a). This design aligns with initial findings from the ITP³³, which used 10-month-old mice to demonstrate lifespan extension with 14.4 ppm 17 α E2 chow. Subsequent studies, involving mice as young as 4 months, report improvements in age-related neuroinflammation^{56,57}. These studies use the UM-HET3 outbred mouse model, which has a longer average lifespan compared to the C57BL/6 background employed in this study⁵⁸. Additionally, previous research showed that in our specific *APOE3* and *APOE4* targeted replacement mouse model, the survival rates at 18 months were 90% and 80%, respectively⁵⁹. Therefore, to assess the effects of 17 α E2 on mitigating age- and *APOE4*-related phenotypes before significant mortality occurred, we initiate treatment at 10 months and conclude the study at 15 months. We first assess the ability of 17 α E2 to mitigate middle-aging phenotypes using (i) a 26-point frailty index³⁸ (Supplementary Data 1A) and (ii) a liver DNA methylation-based epigenetic clock⁶⁰. The frailty index measures visible markers of aging, including the physical/musculoskeletal system, the ocular/nasal system, the respiratory system, the digestive/urogenital system, and observable signs of discomfort³⁸. Notably, we find that control *APOE4* mice have a significantly higher frailty index compared to *APOE3* control, and that *APOE4* mice treated with 17 α E2 have a significantly reduced index that is no longer statistically different from control *APOE3* mice (Fig. 1b; 2-way ANOVA; $F_{\text{treatment}(1,56)} = 5.1$, $p = 0.03$; $F_{\text{genotype}(1,56)} = 5.1$, $p = 0.03$). Using a validated epigenetic clock for mouse aging, we find that *APOE4* animals have a liver DNA methylation signature consistent with that of chronologically relatively older mice, while *APOE3* control and treated mice have a comparatively younger DNA methylation pattern (Fig. 1c; 2-way ANOVA; $F_{\text{genotype}(1,36)} = 12.1$, $p = 0.001$). Note that although the reduced DNA methylation age of 17 α E2-treated *APOE4* mice did not significantly differ from control *APOE4* mice, 17 α E2-treated *APOE4* mice are no longer statistically different from *APOE3* controls, exhibiting a DNA methylation pattern "younger" than their chronological age. Together, these data are consistent with the hypothesis that 17 α E2 treatment initiated at early middle-age leads to improved middle-aging phenotypes specifically in male *APOE4* mice.

17 α E2 decreases body weight and food intake more in male *APOE4* mice

17 α E2 associates with significant reductions in food intake in both the *APOE3* and *APOE4* mice (Figs. 2a, b, 3-way repeated measures ANOVA; $F_{\text{treatment}(1,83)} = 27.7$, $p < 0.0001$) with a statistically nonsignificant trend for a greater effect in *APOE4* (mean $-10.8 \pm 4.5\%$ food intake) than *APOE3* (mean $-4.1 \pm 3.9\%$ food intake) mice. 17 α E2 treatment also results in significant decreases in body weight (Fig. 2c, 3-way repeated measures ANOVA; $F_{\text{treatment}(1,78)} = 46.01$, $p < 0.0001$); however, *APOE4* mice on 17 α E2 display greater reductions (mean $-17.2 \pm 1.8\%$ body weight,) compared to the *APOE3* 17 α E2 treated mice (mean $-6.2 \pm 0.8\%$ body weight). Note that at week 0 of treatment, *APOE4* mice exhibit significantly higher body weight compared to *APOE3* mice (Supplementary Fig. 1a), as well as significantly higher fat mass (Fig. 2d) and lower lean mass (Fig. 2e). Body composition analysis at week 20 reveals a similar pattern of 17 α E2 treatment improvements with both genotypes exhibiting trends for reduced relative fat mass (Fig. 2d, 3-way ANOVA; $F_{\text{treatment}(1,58)} = 8.3$, $p = 0.006$) and increased relative lean mass (Fig. 2e, 3-way ANOVA; $F_{\text{treatment}(1,57)} = 11.3$, $p = 0.001$). There is a non-significant trend of 17 α E2 having a larger effect in *APOE4* mice, with 17 α E2-treated *APOE4* mice having greater reductions of fat mass and more lean mass (Table 1). Importantly, following 17 α E2 treatment, *APOE3* and *APOE4* mice do not significantly differ in measures of body morphometry. These findings are paralleled by tissue weights of visceral and retroperitoneal adipose depots, with reductions reaching statistical significance only in the *APOE4*-treated mice (Supplementary Fig. 1b-c, 2-way ANOVA; visceral: $F_{\text{genotype}(1,58)} = 49.8$, $p < 0.0001$; $F_{\text{treatment}(1,58)} = 18.7$, $p < 0.0001$; retroperitoneal: $F_{\text{genotype}(1,58)} = 11.7$, $p = 0.001$; $F_{\text{treatment}(1,58)} = 24.8$, $p < 0.0001$). Thus, as reported in

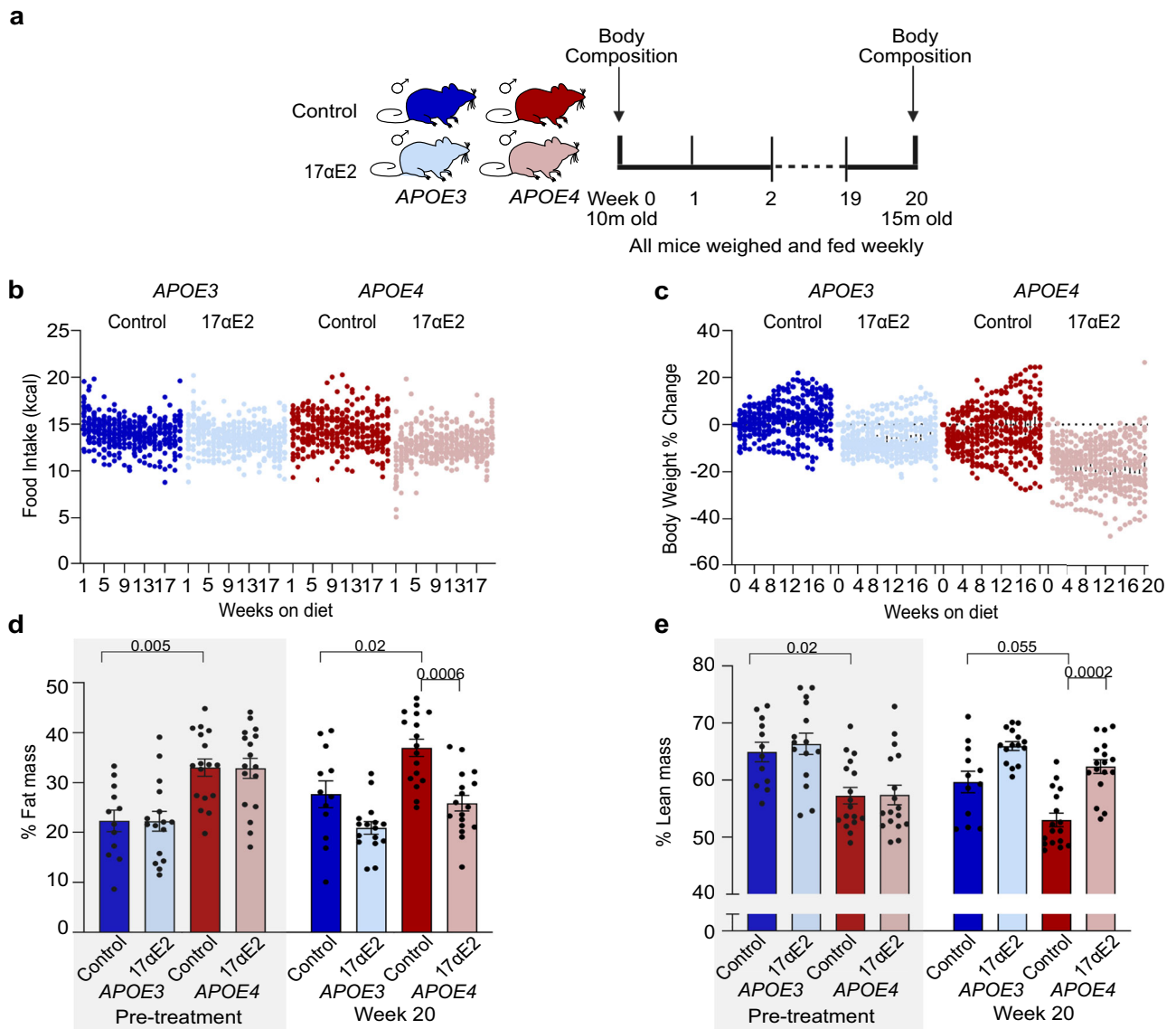


Fig. 2 | 17 α -Estradiol decreases body weight and food intake in middle-aged *APOE3* and *APOE4* targeted-replacement mice. **a** Schematic overview of experimental design. Food intake and body weight were measured weekly. Fat/lean mass was measured at Weeks 0 and 20 of treatment. **b** Food intake (kcal) across the 20 weeks of treatment ($n = 21$ mice/*APOE3* Control, 22/*APOE3* 17 α E2, 21/*APOE4* Control, 23/*APOE4* 17 α E2). **c** Percent body weight change across the 20 weeks of treatment ($n = 19$ mice/*APOE3* Control, 22/*APOE3* 17 α E2, 20/*APOE4* Control, 21/*APOE4* 17 α E2), normalized to weight at Week 0. **d** Fat mass measured by the Bruker Mini Spec ($n = 12$ mice/*APOE3* Control, 16/*APOE3* 17 α E2, 17/*APOE4* Control, 17/*APOE4* 17 α E2). **e** Lean mass measured the Bruker Mini Spec ($n = 12$ mice/*APOE3* Control, 16/*APOE3* 17 α E2, 17/*APOE4* Control, 17/*APOE4* 17 α E2). In **(d)** and **(e)**, shaded panels indicate pre-treatment. In **b** and **c**, dark blue solid lines indicate *APOE3* control, light blue dashed lines indicate *APOE3* 17 α E2, dark red solid lines indicate *APOE4* control, and light red dashed lines indicate *APOE4* 17 α E2. In **d** and **e**, dark blue indicates *APOE3* control, light blue indicates *APOE3* 17 α E2, dark red indicates *APOE4* control, and light red indicates *APOE4* 17 α E2. Data show values from individual animals (**b,c**) with mean \pm SEM (**d,e**). *P*-values denote statistical significance in 2- or 3-way ANOVA with Tukey *post-hoc* test.

genetically heterogeneous mice with wild-type murine *Apoe*²², 17 α E2 associates with reductions in food intake and body weight in mice with knock-in of human *APOE*, though *APOE4* mice experience relatively greater improvements.

17 α E2 improves metabolic measures in targeted replacement *APOE3* and *APOE4* mice

Consistent with the higher adiposity in *APOE4* mice, we find significantly greater hepatic steatosis in control animals with the *APOE4* vs *APOE3* genotype (Fig. 3a, b, Mann-Whitney test, $p = 0.02$). Hepatic steatosis is lower with 17 α E2 treatment in both genotypes, though this effect reaches statistical significance only in *APOE4* mice (Fig. 3b, Mann-Whitney test, $p = 0.005$). In addition to increased fatty liver, *APOE4* control mice exhibit decreased glucose tolerance and

increased plasma leptin (Fig. 3c–e). In the glucose tolerance test, both *APOE3* and *APOE4* mice treated with 17 α E2 display significant improvement (Figs. 3c, d, 2-way ANOVA; $F_{\text{genotype}(1,55)} = 11.6$, $p = 0.001$; $F_{\text{treatment}(1,55)} = 24.2$, $p < 0.0001$). Similar to the outcome of the liver lipid staining, plasma leptin levels are significantly decreased only in the *APOE4*-treated animals (Figs. 3e, 2-way ANOVA; $F_{\text{genotype}(1,42)} = 10.2$, $p = 0.003$; $F_{\text{treatment}(1,42)} = 15.4$, $p = 0.0003$). Thus, our data show that 17 α E2 treatment improves metabolic phenotypes in both male *APOE3* and *APOE4* mice.

17 α E2 reduces genotype-specific differences between *APOE3* and *APOE4* plasma lipidome

As apoE is a key regulator of the lipidome, we next performed shotgun lipidomics on animals from all groups (Fig. 4a). Given the body-wide effects

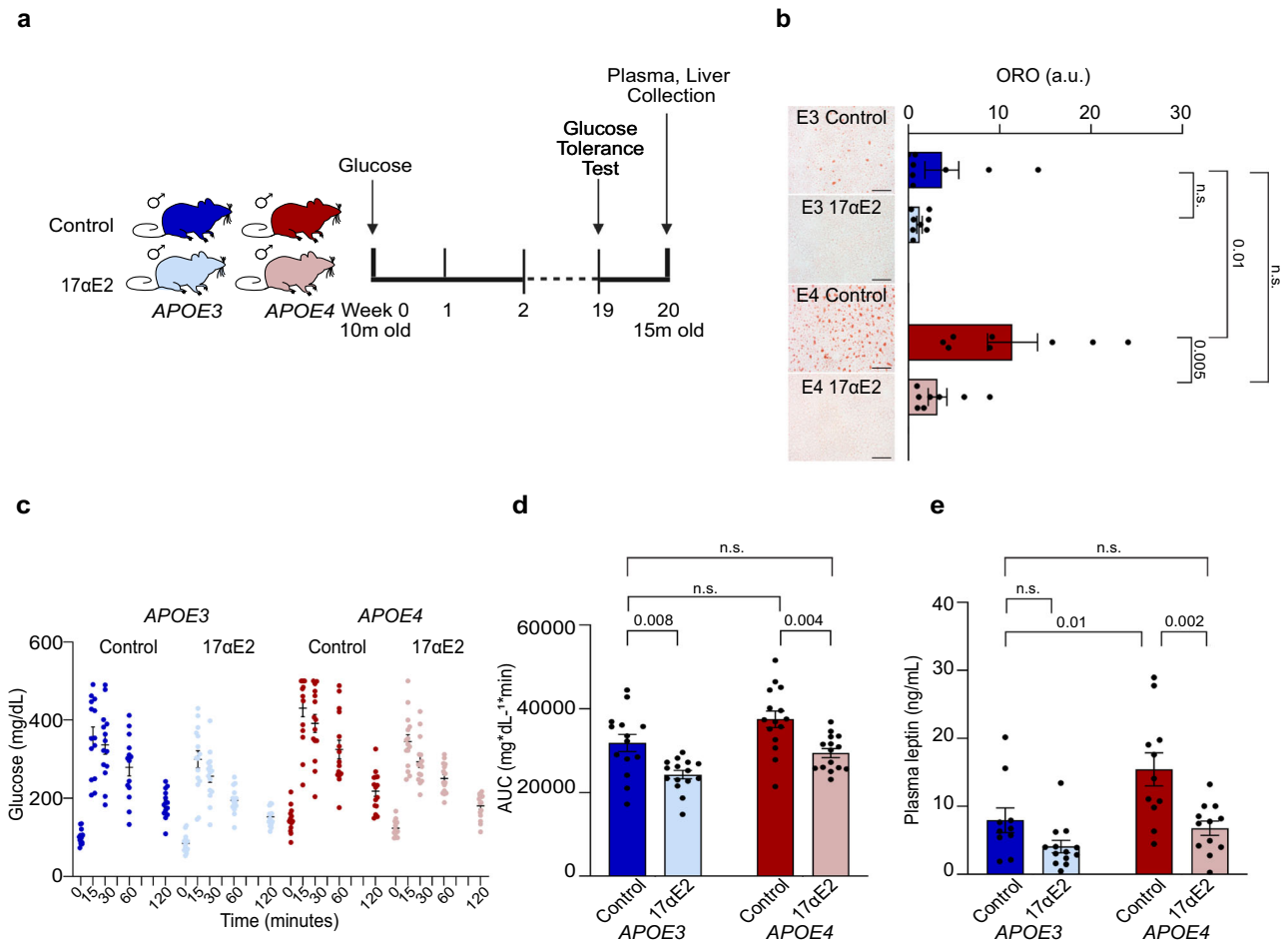


Fig. 3 | 17α-Estradiol improves metabolic outcomes middle-aged APOE3 and APOE4 targeted-replacement mice. **a** Schematic overview of experimental design. Glucose tolerance test was performed at Week 19 of treatment, and tissues were collected at Week 20. **b** Representative images and quantification of oil red O (ORO) labeling of lipid accumulation in livers of 15-month-old male APOE3 and APOE4 mice treated with 0 (Control) or 14.4 ppm 17α-estradiol (17αE2) ($n = 8$ mice/ all groups). Scale bar size indicates 100 μM. **c** Oral glucose tolerance test (GTT) measured at baseline then 15-, 30-, 60-, and 120-minutes post oral gavage with glucose.

d Area under the curve (AUC) analysis for GTT seen in **c** ($n = 14$ mice/APOE3 Control, 15/APOE3 17αE2, 15/APOE4 Control, 15/APOE4 17αE2). **(e)** Plasma levels of leptin measured by ELISA ($n = 10$ mice/APOE3 Control, 13/APOE3 17αE2, 11/APOE4 Control, 12/APOE4 17αE2). Data show values from individual animals (**c**) with mean ± SEM (**b, d, e**). In **b** through **e**, dark blue indicates APOE3 control, light blue indicates APOE3 17αE2, dark red indicates APOE4 control, and light red indicates APOE4 17αE2. *P*-values denote statistical significance in Mann-Whitney test for ORO, 2-way ANOVA with Tukey *post-hoc* test for all other analyses.

of APOE, we analyzed both peripheral (plasma) and neural (cerebral cortex) tissues.

In the plasma (at 15 months-old), we identify 70 lipids with significant differential abundances between APOE3 and APOE4 control mice (Fig. 4b, d, Supplementary Data 2A, FDR < 0.05). This list consists of triglycerides (TG), hexosylceramides (HexCER), and sphingomyelin (SM), among others. Enrichment analysis using LION⁴³ reveals that lipids upregulated in the plasma of APOE4 are primarily involved with endosome/lysosomes and steryl esters, while APOE3 plasma is enriched for lipids involved in lipid storage (Fig. 4c, Supplementary Data 2C). To our knowledge, there are currently no other plasma shotgun lipidomics datasets reported from APOE knock-in mouse models. Compared to previous findings in humans, several lipid types associated with both APOE4 and AD are also significantly differentially regulated in our dataset. Plasma ceramides (CE) CE (17:0), CE (18:0), CE (20:1), CE (22:4), lysophosphatidylcholine (LPC) (20:0), and phosphatidylinositol (PI) (18:0/20:3) are found⁶¹ to be increased in individuals with AD. CE (22:4), CE (24:1), and HexCER (d18:1/22:0) are found to be positively correlated with both APOE4 and AD⁶². In these prior reports^{61,62}, CE (22:4) is positively correlated with AD. Indeed, these AD-associated lipids are all increased in APOE4 control mice. However, between the control APOE3 and 17αE2-treated APOE4 groups there are only three lipids with significant differential abundance, all of which are HexCERs (Fig. 4e,

Supplementary Fig. 2c–e, Supplementary Data 2B, FDR < 0.05). Between APOE3 control and treated groups, as well as between APOE4 control and treated, no significantly different lipids are found, likely because of tissue-specific differences in 17αE2 actions (Supplementary Fig. 2f, g). Finally, an analysis at the level of overall lipid classes reveals a significant interaction between genotype and treatment in CE, with CE increasing with 17αE2 treatment only in APOE3 mice (Supplementary Fig. 2a; 2-way ANOVA; $F_{\text{interaction}(1,14)} = 7.5$, $p = 0.02$; $F_{\text{treatment}(1,14)} = 8.1$, $p = 0.01$). There are significant main effects of both genotype and treatment in HexCER abundance (Supplementary Fig. 2a; 2-way ANOVA; $F_{\text{genotype}(1,14)} = 9.5$, $p = 0.008$; $F_{\text{treatment}(1,14)} = 11.71$, $p = 0.004$). In humans, sphingolipid dysregulation occurs with aging and AD, specifically, increases in long-chain ceramides including HexCER⁶³. Interestingly, increased levels of total HexCER have been reported in a centenarian population⁶⁴. There is also a significant interaction between genotype and treatment in phosphatidic acid (PA), with 17αE2 slightly increasing PA in APOE3-treated mice, while decreasing PA in APOE4 17αE2-treated mice (Supplementary Fig. 2a; 2-way ANOVA; $F_{\text{interaction}(1,14)} = 5.8$, $p = 0.03$). Lastly, there is an overall effect of treatment on phosphatidylcholine (PC) abundance, with 17αE2 increasing PC in both APOE3 and APOE4 mice (Supplementary Fig. 2a; 2-way ANOVA; $F_{\text{treatment}(1,14)} = 4.8$, $p = 0.05$). Taken together, while 17αE2 does not significantly change the individual lipid species content between control and

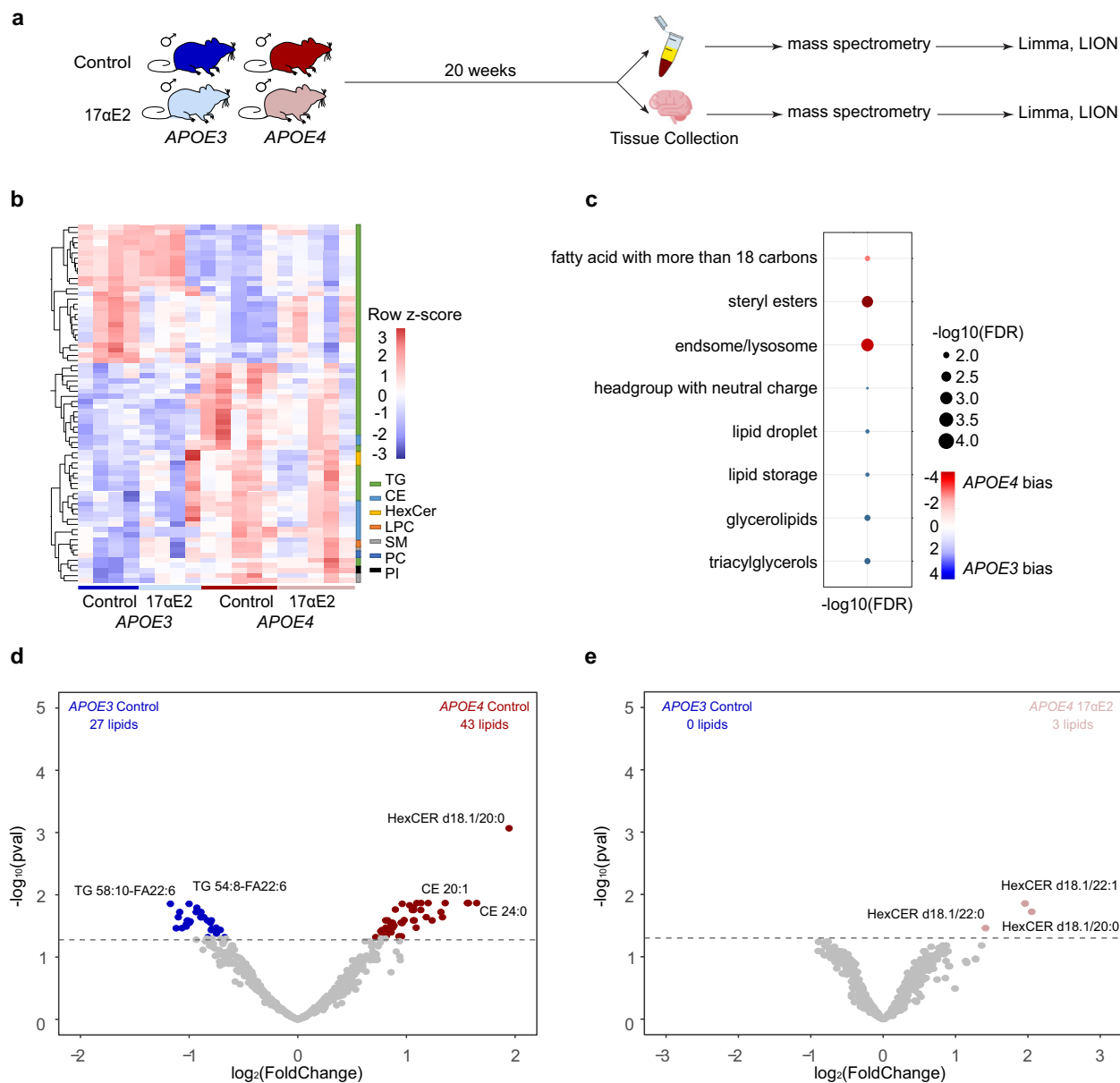


Fig. 4 | 17 α -Estradiol reduces genotype-specific differences in the plasma lipidome of middle-aged APOE3 and APOE4 mice. a Schematic overview of experimental design. Plasma and cerebral cortex were isolated from the RNA-seq cohort after 20 weeks of treatment with Control or 17 α -estradiol (17 α E2). **b** Differentially abundant lipids between APOE3 and APOE4 control mice plasma (FDR 5%) ($n = 4$ mice/APOE3 Control, 4/APOE3 17 α E2, 5/APOE4 Control, 5/APOE4 17 α E2). Red

indicates higher abundance and blue indicates lower abundance. **c** LION lipid ontology analysis of top enriched pathways from the 70 lipids seen in **b**. Red indicates APOE4 bias, blue indicates APOE3 bias. **d** Volcano plot of significantly differentially abundant lipids in APOE3 control versus APOE4 control plasma (FDR 5%). **e** Volcano plot of significantly differentially abundant lipids in APOE3 control versus APOE4 17 α E2 plasma (FDR 5%).

treated groups within APOE genotypes, it does significantly diminish the genotype differences found between APOE3 and APOE4 mice.

In contrast to observations in plasma, we do not find any significant differences in individual lipids based on genotype or 17 α E2 treatment in cerebral cortex tissue. Interestingly, we do find significant APOE genotype differences in overall lipid classes abundances. Specifically, HexCers are significantly increased in APOE4 controls compared to APOE3 controls (Supplementary Fig. 2b, 2-way ANOVA; $F_{\text{genotype}(1,15)} = 10.4$, $p = 0.006$). Previous studies have assessed the cortical lipidome in APOE4 mice using a targeted approach⁶⁵ and, similar to our dataset, found increased amounts of total HexCer in the cortex of APOE4 homozygous mice relative to APOE3 mice⁶⁵. PA levels are decreased in human APOE4 AD patients, and phospholipid dysregulation is strongly implicated in APOE4-associated AD pathogenesis^{66–68}. PA is also increased in both

APOE4 groups compared to APOE3 (Supplementary Fig. 2b, 2-way ANOVA; $F_{\text{genotype}(1,15)} = 9.5$, $p = 0.008$). Sphingomyelin dysregulation is associated with APOE4 and AD^{63,65,69}. Interestingly, sphingomyelin is increased in both groups treated with 17 α E2 (Supplementary Fig. 2b, 2-way ANOVA; $F_{\text{treatment}(1,15)} = 6$, $p = 0.03$).

Collectively, our lipidomic data show that 17 α E2 treatment in male mice dampens APOE genotype-specific differences in the plasma lipidome, with more limited effects in the cerebral cortex.

17 α E2 reduces genotype-specific differences between APOE3 and APOE4 microglia

APOE genotype has established effects on innate immunity and microglia^{70–72}, both of which are also linked to increased risks of cognitive decline and AD. To understand how microglia respond to systemic 17 α E2

treatment in the context of *APOE3* vs. *APOE4* genotypes, we isolated primary microglia from 15-month-old male treated and control mice using magnetic-activated cell sorting (MACS) technology (Fig. 5a). Importantly, these mice were not subjected to any behavioral or metabolic assessments prior to euthanasia, and were processed together to minimize undesired batch effects⁵². Transcriptomes of isolated primary microglia were profiled by RNA-sequencing (RNA-seq) (Fig. 5a).

To assess the similarity of the microglial transcriptomes from our different groups of mice, we first utilize multidimensional scaling (MDS)⁵³. Interestingly, MDS analysis shows clear separation of samples by genotype and treatment (Fig. 5b). Notably, the greatest separation is between *APOE3* and *APOE4* control samples, while the 17αE2-treated groups tend to cluster closer together (Fig. 5b). To further understand the impacts of *APOE* genotype and 17αE2 treatment, we use DESeq2 to reveal transcriptional features with significant genotype- or treatment-related regulation at False Discovery Rate (FDR) < 5% using multivariate linear modeling (Fig. 5c–f, Supplementary Data 3A–D). Importantly, we check the quality of our dataset for appropriate expression of microglia-specific genes, and lack of expression of other common brain cell types (Supplementary Fig. 3a). There are 2,819 genes with significant differential expression between control *APOE3* and *APOE4* microglia; however, when comparing control *APOE3* with 17αE2 *APOE4* microglia, only 652 genes are differentially expressed. When comparing *APOE3* control and treated groups, there are 1016 differentially expressed genes. Only 37 differentially expressed genes are identified between control and treated *APOE4* groups, suggesting a larger effect on the microglia transcriptome in the *APOE3* animals. Interestingly, comparison of transcriptome-wide changes show that 17αE2 treatment in *APOE3* mice associates with acquisition of a more *APOE4*-like transcriptional landscape, with very few genes changing in the same direction across both genotypes (Supplementary Fig. 3b–d). This comparison also reveals that 17αE2 *APOE4* microglia have a transcriptional landscape more similar to *APOE3* control microglia (Supplementary Fig. 3e).

Next, we ask which functional Gene Ontology gene sets are regulated by 17αE2 treatment within the *APOE3* and *APOE4* groups. Looking at the top 5 up- and down-regulated significantly changed gene sets per genotype upon 17αE2 treatment, we find gene sets both similarly and divergently regulated by 17αE2 in the *APOE3* and *APOE4* groups. Sets similarly regulated by 17αE2 include those relating to sensory reception, “haptoglobin-hemoglobin complex”, “negative regulation of activated T cell proliferation”, and “taurine transport”. Haptoglobin and hemoglobin are both implicated in microglia-related inflammation, with studies suggesting haptoglobin regulates microglia-induced inflammation⁷³. Intriguingly, a recent study reported that taurine is crucial to healthy aging, and deficiency drives middle-aging phenotypes⁷⁴ (Fig. 5g). Divergently regulated gene sets include “cilium movement”, “microtubule bundle formation”, and “extracellular transport”, with these being upregulated in the *APOE4* 17αE2-treated group (Fig. 5h). The *APOE3* 17αE2-treated group shows upregulation of gene sets relating to “condensed chromosome outer kinetochore”, “activation of innate immune-response”, “RISC complex”, “RNAi effector complex”, and “negative regulation of interleukin-10 production” (Fig. 5h). Thus, while 17αE2 treatment appears to affect the microglia transcriptome differently between *APOE3* and *APOE4* mice, both genotypes exhibit changes in gene sets relating to metabolic/immune system processes.

Effects of 17αE2 on neural measures in targeted replacement *APOE3* and *APOE4* mice

After 15 weeks of 17αE2 treatment, animals from all groups were subjected to behavioral assessments (Fig. 6a). To measure effects of *APOE* and 17αE2 treatment on general measures of motor activity and anxiety, mice were assessed in the open field task. There are no significant differences across the groups in the time spent exploring the center of the field (Supplementary Fig. 4a) although there is a significant genotype effect in the total distance

traveled with *APOE4* animals showing higher levels (Supplementary Fig. 4b). There are no significant main effects of genotype or treatment on behavioral performance in tasks of exploratory behavior and short-term spatial memory (spontaneous alternation behavior in the Y-maze; Supplementary Fig. 4c) and spatial recognition memory (novel object placement; Supplementary Fig. 4e). However, there is a significant interaction between genotype and treatment in novel object recognition, with 17αE2 improving performance only in *APOE4* mice (Supplementary Fig. 4d, 2-way ANOVA; $F_{\text{Interaction}(1, 40)} = 7.14, p = 0.01$).

In the Barnes maze test of spatial learning and memory, we observe *APOE4*-associated deficits, consistent with previous findings from other groups⁷⁵. In this task, evidence of learning over successive days of trials is indicated by shorter latencies and path lengths in reaching the target as well as reductions in the number of errors in choosing the target. Escape latencies show significant main effects for time (Figs. 6b, 3-way ANOVA; $F_{\text{time}(2.5, 116.1)} = 8.02, p = 0.0002$) and genotype (Figs. 6b, 3-way ANOVA; $F_{\text{time}(1, 46)} = 4.06, p = 0.05$), which indicate learning by all groups but poorer performance by *APOE4* mice (Fig. 6b). There are significant reductions in primary path lengths across groups (Figs. 6c, 3-way ANOVA; $F_{\text{time}(2.7, 123.6)} = 8.05, p = 0.0001$), consistent with learning. *APOE4* mice show a nonsignificant trend of shorter path lengths, however relative levels of reduction over the training days (i.e., learning) trend in favor of *APOE3* mice (control: 20.4% ± 9.1, 17αE2: 17.4% ± 7.7 reductions) versus *APOE4* mice (control: 10.3% ± 6.5, 17αE2: 5.2% ± 3.7 reductions). Neither latency nor path length are significantly impacted by 17αE2 treatment. Error number shows a significant interaction between time and *APOE* genotype (Figs. 6d, 3-way ANOVA; $F_{\text{time} \times \text{genotype}(3, 138)} = 7.8, p < 0.0001$). Specifically, both *APOE3* groups have decreased errors over training days, whereas *APOE4* mice show divergent patterns with performance slightly worsening in *APOE4* control mice and improving in *APOE4* treated mice (Fig. 6d). Error number shows a similar pattern on the probe trial: significantly more errors are observed in control but not treated *APOE4* mice relative to control *APOE3* mice (Figs. 6e, 2-way ANOVA Tukey’s multiple comparisons; $p = 0.01$). These findings are consistent with previous studies that show *APOE4* mice perform worse than *APOE3* on tasks like the Morris water maze, which tests similar hippocampal-dependent memory as the Barnes maze, and novel object recognition task⁷⁶. Together, the Barnes maze data are consistent with prior reports of deficits in spatial learning and memory performance in *APOE4* mice^{10,77} and suggest partial functional improvements with 17αE2 treatment in terms of error level.

As both *APOE*^{72,66,77–81} and 17αE2^{14,17–19,24} exert a range of effects on the brain, we also considered additional neural outcomes. First, we considered measures of gliosis. We quantified immunohistochemical burden of markers for both astrogliosis (glial fibrillary acid protein) and microgliosis (ionized calcium binding adaptor molecule 1), established measures of states of glial response^{82,83}. In the CA1 region of the hippocampus, we observe a modest but significant effect of genotype on astrogliosis, with *APOE4* mice having higher levels than *APOE3* mice (Supplementary Fig. 4f, 2-way ANOVA; $F_{\text{genotype}(1, 23)} = 5.12, p = 0.03$). There is a non-significant trend for an overall effect of treatment to reduce astrogliosis load ($p = 0.09$) (Supplementary Fig. 4f). We find no significant differences in microglial burden across the groups (Supplementary Fig. 4g).

Next, we examined levels of brain oxidation by measuring 4-hydroxynonenal (4HNE), a product of lipid peroxidation and biomarker of oxidative stress⁸⁴. Lipid peroxidation is observed with normal brain aging and further in AD^{84–87} and is particularly strong in lipid rafts. Indeed, recent evidence in human samples shows that 4HNE levels in cerebrocortical lipid rafts are robustly elevated by both *APOE4* and AD⁸⁷. Consistent with these data, we see significantly higher 4HNE in cerebrocortical lipid rafts from *APOE4* control mice relative to the *APOE3* controls (Figs. 6f, 2-way ANOVA Tukey’s multiple comparisons; $p = 0.03$). Notably, there is a significant treatment X genotype interaction (Figs. 6f, 2-way ANOVA; $F_{\text{interaction}(1, 36)} = 11.6, p = 0.002$) in which 17αE2 treatment induces significant decreases in 4HNE levels in *APOE4* but not *APOE3* mice.

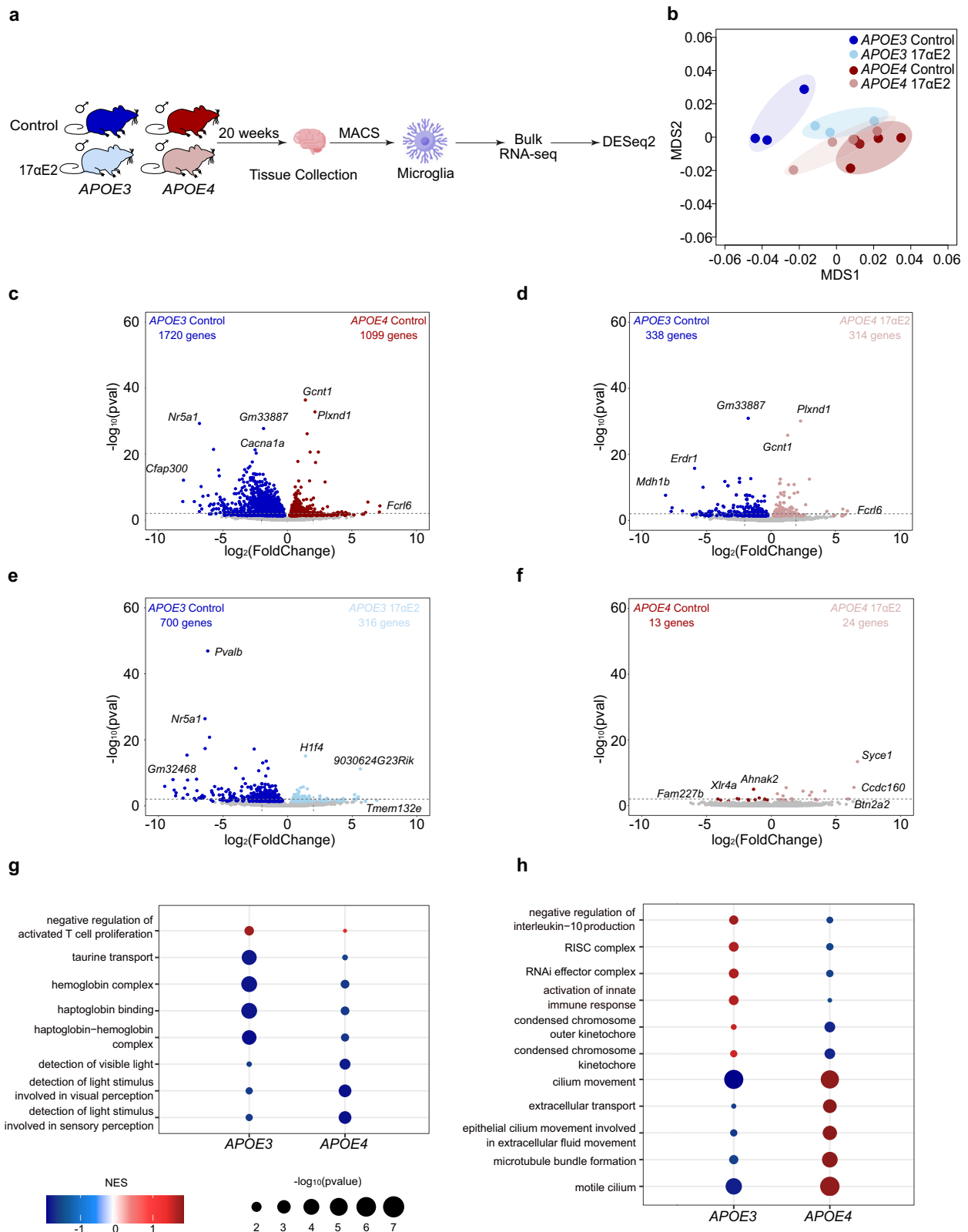


Fig. 5 | 17 α -Estradiol reduces genotype-specific differences in the microglia transcriptomes of APOE3 and APOE4 mice. **a** Schematic overview of experimental design. Microglia were isolated from the RNA-seq cohort at Week 20. **b** Multi-dimensional scaling (MDS) of transcriptomes for microglia from all four groups ($n = 3$ mice/APOE3 Control, 3/APOE3 17 α E2, 5/APOE4 Control, 4/APOE4 17 α E2). **c** Volcano plot of differentially expressed genes (DESeq2 FDR < 5%) between APOE3 control (dark blue) and APOE4 control (dark red) microglia. **d** Volcano plot of differentially expressed genes (FDR < 5%) between APOE3 control (dark blue) and APOE3 17 α E2 (light blue) microglia. **e** Volcano plot of differentially expressed genes (FDR < 5%) between APOE3 control (dark blue) and APOE4 17 α E2 (light red) microglia. **f** Volcano plot of differentially expressed genes (FDR < 5%) between APOE4 control (dark red) and APOE4 17 α E2 (light red) microglia. **g** Effect of 17 α E2 in APOE3 and APOE4 microglia gene set enrichment analysis (gene ontology). Bubble plot shows top similarly changed gene sets (DESeq2 FDR < 5%). **h** Effect of 17 α E2 in APOE3 and APOE4 microglia gene set enrichment analysis (gene ontology). The bubble plot shows top divergently changed gene sets (DESeq2 FDR < 5%).

and APOE4 17 α E2 (light red) microglia. **e** Volcano plot of differentially expressed genes (FDR < 5%) between APOE3 control (dark blue) and APOE3 17 α E2 (light blue) microglia. **f** Volcano plot of differentially expressed genes (FDR < 5%) between APOE4 control (dark red) and APOE4 17 α E2 (light red) microglia. **g** Effect of 17 α E2 in APOE3 and APOE4 microglia gene set enrichment analysis (gene ontology). Bubble plot shows top similarly changed gene sets (DESeq2 FDR < 5%). **h** Effect of 17 α E2 in APOE3 and APOE4 microglia gene set enrichment analysis (gene ontology). The bubble plot shows top divergently changed gene sets (DESeq2 FDR < 5%).

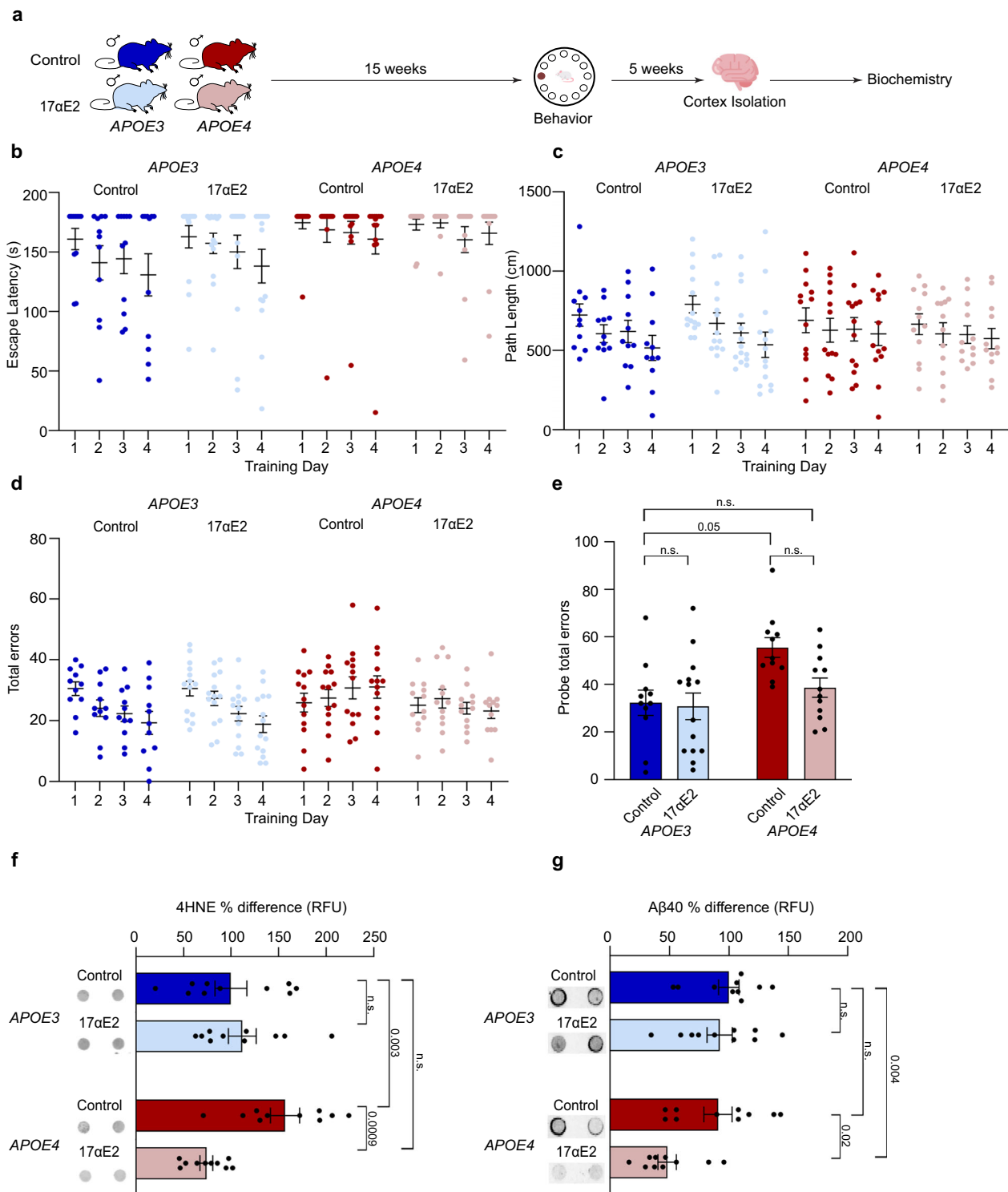


Fig. 6 | 17 α -Estradiol yields greater neural benefits in $APOE4$ mice than $APOE3$ mice. **a** Schematic overview of experimental design. Animals were subjected to behavior tests after 15 weeks of treatment. One hemibrain was fixed for immunohistochemistry, and the cerebral cortex from the other hemibrain was isolated for protein extraction. **b** Escape latency during the Barnes maze training days ($n = 11$ mice/ $APOE3$ Control, 14/ $APOE3$ 17 α E2, 13/ $APOE4$ Control, 12/ $APOE4$ 17 α E2). **c** Primary path length to escape hole during the Barnes maze training days ($n = 11$ mice/ $APOE3$ Control, 14/ $APOE3$ 17 α E2, 13/ $APOE4$ Control, 12/ $APOE4$ 17 α E2). **d** Total errors during the Barnes maze training days ($n = 11$ mice/ $APOE3$ Control, 14/ $APOE3$ 17 α E2, 13/ $APOE4$ Control, 12/ $APOE4$ 17 α E2).

e Total errors during the Barnes maze probe trial ($n = 11$ mice/ $APOE3$ Control, 14/ $APOE3$ 17 α E2, 11/ $APOE4$ Control, 12/ $APOE4$ 17 α E2). **f** Quantification of the lipid peroxidation marker 4-hydroxynonenal (4-HNE) from cortical lipid rafts and representative dot blot images ($n = 10$ mice/ all groups). **g** Quantification of soluble β -amyloid peptide ($A\beta_{40}$) from cortical homogenates and representative dot blot images ($n = 10$ mice/ all groups). In **b** through **g**, dark blue indicates $APOE3$ control, light blue indicates $APOE3$ 17 α E2, dark red indicates $APOE4$ control, and light red indicates $APOE4$ 17 α E2. Data show values from individual animals (**b, c, d**) with mean \pm SEM (**e, f, g**). P -values denote statistical significance in 2-way ANOVA with Tukey *post-hoc* test.

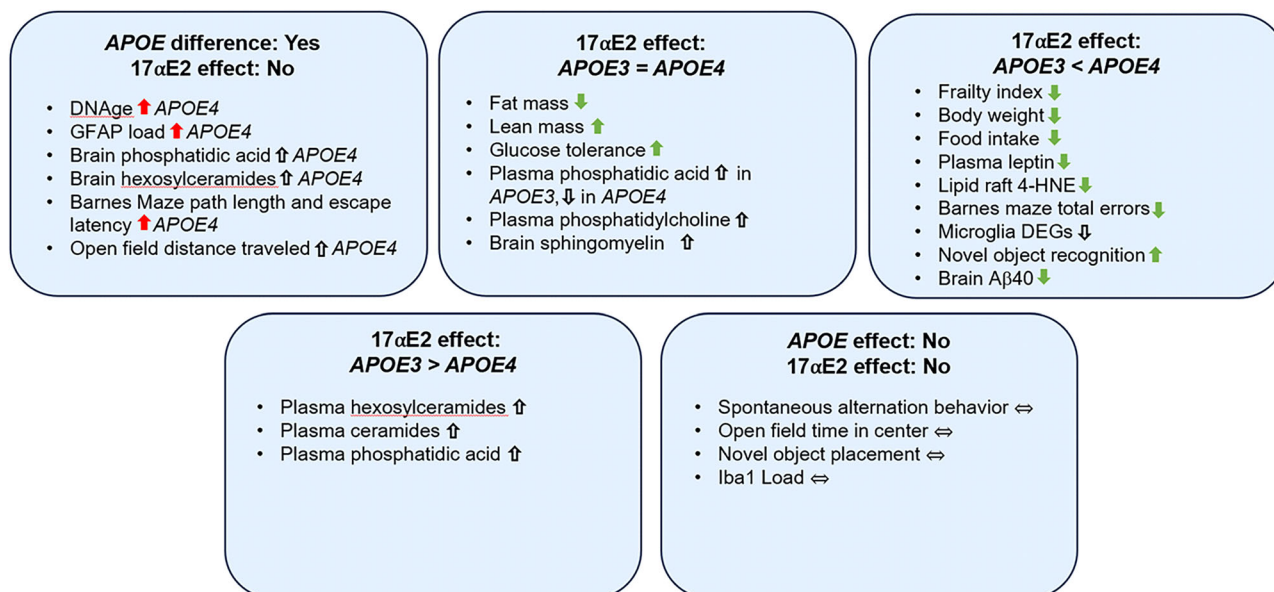


Fig. 7 | Classification of outcomes based on genotype and treatment. Outcomes are categorized into five groups: (i) significant genotype differences with no significant effects of 17α-estradiol (17αE2) treatment, (ii) outcomes improved by 17αE2 treatment in both *APOE3* and *APOE4* mice, (iii) outcomes changed by 17αE2

treatment only or more strongly in *APOE4* mice, (iv) outcomes changed by 17αE2 treatment only or more strongly in *APOE3* mice, and (v) outcomes with no significant genotype or treatment effects.

Next, we measured levels of amyloid-beta ($A\beta$), a protein implicated in AD pathogenesis, in cerebral cortex homogenates using a dot blot technique⁵⁵. We find that 17αE2 treatment associates with a significant reduction in cerebrocortical $A\beta_{x-40}$ in *APOE4* but not *APOE3* mice (Figs. 6g, 2-way ANOVA; $F_{\text{treatment}(1,36)} = 6.5$, $p = 0.02$, $F_{\text{genotype}(1,36)} = 7.4$, $p = 0.01$). Taken together, we see that *APOE4* genotype associates with select deficits in cognition, increased gliosis, and increased lipid peroxidation, which are partially attenuated by 17αE2 treatment.

Discussion

APOE genotype associates with body-wide changes in lipids, inflammatory tone, and metabolism that are widely posited to underlie its relationships with increased risks of mortality, cognitive impairment, and AD. Here, we investigate the hypothesis that interventions established to promote healthspan and longevity may be particularly efficacious against the systemic progeroid phenotypes of *APOE4*. Our findings demonstrate that treatment with the longevity-promoting compound 17αE2 during early middle age protects against the development of middle-aging phenotypes often in an *APOE* genotype-specific manner. Across aging, metabolic, and behavioral measures, we find a similar trend: *APOE4* mice are impaired compared to *APOE3*, and this difference is largely attenuated by 17αE2 such that treated *APOE4* mice appear similar to untreated *APOE3* mice. This is consistent when looking at morphological and epigenetic markers of aging (Fig. 1), body mass composition (Fig. 2), hepatic steatosis, plasma leptin (Fig. 3), the Barnes maze behavioral task, and brain lipid peroxidation (Fig. 6). 17αE2-induced improvements in metabolic measures in aging male mice were previously reported^{21,22,27}, but, to the best of our knowledge, our findings are the first to demonstrate that these improvements are significantly influenced by *APOE* genotype, a genetic factor associated with aging, longevity, and AD^{24,12}. 17αE2-treated *APOE4* mice have improvements in all metabolic parameters measured. In the Barnes maze task of spatial learning and memory, 17αE2-treated *APOE4* mice significantly reduce their total errors, making them statistically indistinguishable from the *APOE3* mice. 17αE2 treatment in *APOE4* mice also associates with significantly lower cerebrocortical levels of $A\beta$, a protein implicated as a central factor in AD pathogenesis. Collectively, these findings suggest 17αE2 treatment could be a potential therapeutic against middle-aged phenotypes,

including increased vulnerability to age-related cognitive decline and AD, particularly in the context of *APOE4* genotype.

In our analysis, we categorize outcomes into five distinct groups based on their responses to genotype and 17αE2 treatment (Fig. 7). The first group includes outcomes where significant differences were observed between *APOE4* and *APOE3* mice, but 17αE2 treatment does not significantly improve *APOE4*-associated phenotypes. These outcomes include DNAge, GFAP load, brain lipids (PA and HexCer), distance traveled in the open field test, and Barnes maze measures such as path length and escape latency. The second group comprises outcomes where 17αE2 treatment has similar effects on both *APOE3* and *APOE4* mice, including body composition, glucose tolerance, plasma PC, and brain SM. Notably, plasma PA exhibited a differential response, increasing in *APOE3* 17αE2-treated mice but decreasing in *APOE4* 17αE2-treated mice. The third group consists of outcomes where 17αE2 treatment specifically affects *APOE4* mice, such as frailty, body weight, total errors in the Barnes maze, brain $A\beta_{x-40}$ levels, and other measures. In contrast, the fourth group includes outcomes where 17αE2 treatment only influences *APOE3* mice, such as plasma Cer, HexCer, and PA. Finally, the fifth group contains outcomes that show no significant effects of either genotype or 17αE2 treatment. These include spontaneous alternation behavior, time spent in the center of the open field test, novel object placement, and Iba1 load. Overall, there is variability in 17αE2 effects based on outcome and genotype, with some efficacy seen in mitigating *APOE4*-associated differences but limited or adverse effects, particularly in *APOE3* mice. This reflects the potential of 17αE2 as a targeted intervention while also highlighting the need to carefully assess its differential effects across genetic backgrounds.

The mechanism(s) contributing to the moderating effects of *APOE* genotype on 17αE2 treatment remain to be determined. One potential mechanism by which 17αE2 may be eliciting genotype-specific effects is related to reported differences in levels of estrogen receptors by *APOE* genotype. Interestingly, female EFAD mice that carry *APOE4* show significantly higher estrogen receptor α (ER α) levels in the dorsal hippocampus⁸⁸. A similar observation was reported in female *APOE4*-targeted replacement mice without the 5xFAD transgene⁷⁰. Prior work indicates that 17αE2 primarily acts through ER α ²⁹, which suggests that its efficacy may be enhanced with elevated ER α expression. In this case, relatively higher ER α in *APOE4* mice may

play a role in the observed selective benefits of 17 α E2 seen in *APOE4* mice.

Given the robust evidence that longevity interventions can slow declines in tissue function associated with normal aging that begins in early adulthood and becomes more pronounced by midlife^{89,90}, they hold significant promise as protective measures against numerous age-related diseases. Notably, many longevity interventions not only extend lifespan, but also lessen metabolic dysfunction, indicating a complex interplay between longevity and metabolic integrity^{13,22,31}. Metabolic dysfunction and diseases such as diabetes and hypertension are known drivers of aging phenotypes, cognitive decline, and AD, acting through mechanisms including systemic inflammation^{91,92}. *APOE4* is linked to metabolic dysfunction^{5,10,11,68}, which may contribute to its relationships with aging processes and age-related diseases. Older adults with *APOE4* are more likely to experience brain glucose hypometabolism, atherosclerosis, and ischemic heart disease⁹³. *APOE4* genotype significantly impacts longevity, with most^{4,94,95} but not all⁹⁶ studies associating *APOE4* with increased mortality. Our findings, consistent with existing research, support the notion that *APOE4* induces “pro-aging” phenotypes in both humans and mice^{4,94,95}. Given that *APOE4* carrier status is observed in ~15% of the U.S. population⁷⁷ and in ~60% of AD patients⁶, there is a significant need to identify interventions that can mitigate the heightened risks associated with *APOE4*. This study focuses on 17 α E2 as a proof-of-principle intervention, leveraging its well-established multi-system protective effects. We sought to explore 17 α E2’s potential in addressing the multifaceted challenges posed by *APOE4*, offering insights for intervention that may extend beyond metabolic health to encompass neuroprotection.

Our research, in conjunction with other studies^{13,31}, highlights that longevity drugs are not a “one-size-fits-all” approach to treating age-related impairments and reducing risks for disease. Indeed, a variety of factors interplay in drug responsiveness, including age, genetics, and sex dimorphisms. Our specific findings on 17 α E2 reveal differential impact in *APOE3* and *APOE4* male mice, with significant protection in *APOE4* mice but a slightly beneficial to neutral effect in *APOE3* male mice. This genotype-dependent effect suggests that the progeroid phenotypes associated with *APOE4* may be especially responsive to longevity-related interventions. Alternative strategies may prove more effective in an *APOE3* context, highlighting the importance of exploring diverse approaches tailored to specific genetic backgrounds. In human pharmacokinetics, the interplay between age and genotype introduces complexities, with advancing age resulting in almost a 1.5-fold increase in systemic exposure to certain drugs, influenced by specific genotypes⁹⁷. Biological sex adds an additional complexity on top of age and genotype. Longevity interventions exhibit robust sex dimorphism, with many interventions demonstrating more pronounced efficacy in males. This observation calls for future studies in geroprotection to actively seek out drugs with positive effects in females, especially in the context of diseases such as AD that have a significant female bias⁹⁸. Our study contributes to the growing understanding that genotype plays a pivotal role in determining the optimized responsiveness of interventions for age-related conditions. This aligns with the overarching concept of personalized medicine, emphasizing the need for individualized approaches that consider genetic profiles as one of several important factors to optimize therapeutic outcomes^{99,100}.

In summary, we find that 17 α E2 improves a range of systemic and neural outcomes in an *APOE*-dependent manner. Specifically, the health-span benefits of 17 α E2 are observed more in *APOE4* mice, a genotype that generally associates with poorer mortality and aging outcomes in both mice and humans. Treatment with 17 α E2 improves frailty, metabolic parameters, and plasma lipidome profiles in a genotype-dependent manner, with greater benefits observed in *APOE4* mice and more limited effects on *APOE4* cortical lipidome, microglial transcriptome, and cognitive function. In *APOE3* mice, the metabolic benefits are modest, and their microglial transcriptome and plasma lipidome profiles shift toward an *APOE4*-like pattern with 17 α E2 treatment. Additionally, no cognitive or neural benefits are observed in *APOE3* mice. The ability of 17 α E2 to alleviate adverse phenotypes across multiple systems linked to *APOE4* genotype implies that 17 α E2

might offer mitigation of the *APOE4*-associated risks, including cognitive decline and AD.

There are a few limitations to this study. First, only male mice were studied, thus the observed *APOE* genotype-dependent effects of 17 α E2 may differ in females. As the effects of *APOE4* interact with sex in both humans^{101,102} and rodents^{103,104}, future research should specifically explore the effects of 17 α E2 in female mice with human *APOE3* and *APOE4* despite the absence of significant longevity promotion by 17 α E2 in female mice¹³. Second, mouse strain can affect the efficacy of longevity-promoting promoting interventions^{105,106}. It is noteworthy that the key studies of 17 α E2 on longevity employed UM-HET3 mice^{13,31}, while mice on a predominantly C57BL/6 background were utilized in this study. Strain-specific variations may reasonably influence the findings observed in *APOE3* and *APOE4* humanized mice. Third, *APOE* allele zygosity may be important to 17 α E2 effects. Our group recently published findings in female *APOE* mice on the impact of *APOE* zygosity on responses to obesogenic diet and estradiol treatment. We found that *APOE3/4* heterozygous mice often displayed intermediate responses relative to *APOE3/3* and *APOE4/4* homozygotes, particularly in measures like microglial density, response state, and neurogenesis. *APOE3/4* mice also exhibited distinct profiles in specific outcomes: metabolic responses tended to resemble those of *APOE3*, while behavioral responses were more similar to *APOE4*. These findings indicate that *APOE3/4* heterozygosity can produce unique patterns of estrogen responsiveness¹⁰⁷ and should be investigated further with respect to 17 α E2. Additionally, we use 15-month-old mice in our study and, although cognitive deficits and neuroinflammation have been documented at this and earlier timepoints in this model, the use of older mice may more effectively capture age-related neural impairments. Lastly, although our study implies a potential protective role of 17 α E2 against *APOE4*-associated cognitive decline and AD risk, this research does not directly address AD pathology. Further investigation of 17 α E2 effects in the presence of AD-related pathways and factors, such as amyloidosis and tauopathy, should be pursued in additional rodent models to establish a more comprehensive understanding across the complexities of AD in humans.

Reporting summary

Further information on research design is available in the Nature Portfolio Reporting Summary linked to this article.

Data availability

The source data for Figs. 1, 2, 3 and 6 and Supplementary Figs. 1, 2, 5 and 6 are in Supplementary Data 4. All sequencing data were deposited to the SRA under accession PRJNA1078754. Lipidomics (<https://doi.org/10.6084/m9.figshare.25346143>)¹⁰⁸ and DNAGE (<https://doi.org/10.6084/m9.figshare.25386586>)¹⁰⁹ data were deposited to FigShare. All other data are available from the corresponding author upon reasonable request.

Code availability

All R scripts are available on GitHub repository. https://github.com/BenayounLaboratory/17aE2_APOE (<https://doi.org/10.5281/zenodo.15474598>)¹¹⁰.

Received: 11 April 2024; Accepted: 30 May 2025;

Published online: 10 June 2025

References

1. Brito, D. V. C. et al. Assessing cognitive decline in the aging brain: lessons from rodent and human studies. *NPJ Aging* **9**, 23 (2023).
2. Michaelson, D. M. *APOE* ϵ 4: the most prevalent yet understudied risk factor for Alzheimer’s disease. *Alzheimers Dement.* **10**, 861–868 (2014).
3. Serrano-Pozo, A., Das, S. & Hyman, B. T. *APOE* and Alzheimer’s disease: advances in genetics, pathophysiology, and therapeutic approaches. *Lancet Neurol.* **20**, 68–80 (2021).
4. Shinohara, M. et al. *APOE2* is associated with longevity independent of Alzheimer’s disease. *Elife* **9**, e62199 (2020).

5. Johnson, L. A. APOE and metabolic dysfunction in Alzheimer's disease. *Int. Rev. Neurobiol.* **154**, 131–151 (2020).
6. Ward, A. et al. Prevalence of apolipoprotein E4 genotype and homozygotes (APOE ϵ 4/4) among patients diagnosed with Alzheimer's disease: a systematic review and meta-analysis. *Neuroepidemiology* **38**, 1–17 (2012).
7. Marais, A. D. Apolipoprotein E in lipoprotein metabolism, health and cardiovascular disease. *Pathology* **51**, 165–176 (2019).
8. Martínez-Martínez, A. B. et al. Beyond the CNS: The many peripheral roles of APOE. *Neurobiol. Dis.* **138**, 104809 (2020).
9. Rebeck, G. W. The role of APOE on lipid homeostasis and inflammation in normal brains. *J. Lipid Res.* **58**, 1493–1499 (2017).
10. Johnson, L. A., Torres, E. R., Impey, S., Stevens, J. F. & Raber, J. Apolipoprotein E4 and Insulin Resistance Interact to Impair Cognition and Alter the Epigenome and Metabolome. *Sci. Rep.* **7**, 43701 (2017).
11. Johnson, L. A. et al. Apolipoprotein E4 mediates insulin resistance-associated cerebrovascular dysfunction and the post-prandial response. *J. Cereb. Blood Flow. Metab.* **39**, 770–781 (2019).
12. Martens, Y. A. et al. ApoE Cascade Hypothesis in the pathogenesis of Alzheimer's disease and related dementias. *Neuron* **110**, 1304–1317 (2022).
13. Harrison, D. E. et al. Acarbose, 17- α -estradiol, and nordihydroguaiaretic acid extend mouse lifespan preferentially in males. *Aging Cell* **13**, 273–282 (2014).
14. Barha, C. K., Dalton, G. L. & Galea, L. A. Low doses of 17 α -estradiol and 17 β -estradiol facilitate, whereas higher doses of estrone and 17 α - and 17 β -estradiol impair, contextual fear conditioning in adult female rats. *Neuropsychopharmacology* **35**, 547–559 (2010).
15. Gonzalez-Freire, M., Diaz-Ruiz, A. & de Cabo, R. 17 α -Estradiol: A novel therapeutic intervention to target age-related chronic inflammation. *J. Gerontol. A Biol. Sci. Med. Sci.* **72**, 1–2 (2017).
16. Kaur, S. P., Bansal, S. & Chopra, K. 17 α -Estradiol: a candidate neuroserm and non-feminizing estrogen for postmenopausal neuronal complications. *Steroids* **96**, 7–15 (2015).
17. MacLusky, N. J., Luine, V. N., Hajszan, T. & Leranth, C. The 17 α and 17 β isomers of estradiol both induce rapid spine synapse formation in the CA1 hippocampal subfield of ovariectomized female rats. *Endocrinology* **146**, 287–293 (2005).
18. McClean, J. & Nuñez, J. L. 17 α -Estradiol is neuroprotective in male and female rats in a model of early brain injury. *Exp. Neurol.* **210**, 41–50 (2008).
19. Ozacmak, V. H. & Sayan, H. The effects of 17 β estradiol, 17 α estradiol and progesterone on oxidative stress biomarkers in ovariectomized female rat brain subjected to global cerebral ischemia. *Physiol. Res.* **58**, 909–912 (2009).
20. Shughrue, P. J. & Merchenthaler, I. Estrogen prevents the loss of CA1 hippocampal neurons in gerbils after ischemic injury. *Neuroscience* **116**, 851–861 (2003).
21. Steyn, F. J. et al. 17 α -estradiol acts through hypothalamic pro-opiomelanocortin expressing neurons to reduce feeding behavior. *Aging Cell* **17**, e12703 (2018).
22. Stout, M. B. et al. 17 α -Estradiol alleviates age-related metabolic and inflammatory dysfunction in male mice without inducing feminization. *J. Gerontol. A Biol. Sci. Med. Sci.* **72**, 3–15 (2017).
23. Korenman, S. G. Comparative binding affinity of estrogens and its relation to estrogenic potency. *Steroids* **13**, 163–177 (1969).
24. Dykens, J. A., Moos, W. H. & Howell, N. Development of 17 α -estradiol as a neuroprotective therapeutic agent: rationale and results from a phase I clinical study. *Ann. N. Y. Acad. Sci.* **1052**, 116–135 (2005).
25. Liu, R. et al. 17 β -Estradiol attenuates blood-brain barrier disruption induced by cerebral ischemia-reperfusion injury in female rats. *Brain Res.* **1060**, 55–61 (2005).
26. Perez, E. et al. Neuroprotective effects of an estratriene analog are estrogen receptor independent in vitro and in vivo. *Brain Res.* **1038**, 216–222 (2005).
27. Garratt, M., Bower, B., Garcia, G. G. & Miller, R. A. Sex differences in lifespan extension with acarbose and 17- α estradiol: gonadal hormones underlie male-specific improvements in glucose tolerance and mTORC2 signaling. *Aging Cell* **16**, 1256–1266 (2017).
28. Garratt, M. et al. Male lifespan extension with 17- α estradiol is linked to a sex-specific metabolomic response modulated by gonadal hormones in mice. *Aging Cell* **17**, e12786 (2018).
29. Mann, S. N. et al. Health benefits attributed to 17 α -estradiol, a lifespan-extending compound, are mediated through estrogen receptor α . *Elife* **9**, e59616 (2020).
30. Sidhom, S. et al. 17 α -Estradiol modulates IGF1 and hepatic gene expression in a sex-specific manner. *J. Gerontol. A Biol. Sci. Med. Sci.* **76**, 778–785 (2021).
31. Strong, R. et al. Longer lifespan in male mice treated with a weakly estrogenic agonist, an antioxidant, an α -glucosidase inhibitor or a Nrf2-inducer. *Aging Cell* **15**, 872–884 (2016).
32. Youmans, K. L. et al. APOE4-specific changes in A β accumulation in a new transgenic mouse model of Alzheimer disease. *J. Biol. Chem.* **287**, 41774–41786 (2012).
33. Harrison, D. E. et al. 17- α -estradiol late in life extends lifespan in aging UM-HET3 male mice; nicotinamide riboside and three other drugs do not affect lifespan in either sex. *Aging Cell* **20**, e13328 (2021).
34. Hughes, R. N. The value of spontaneous alternation behavior (SAB) as a test of retention in pharmacological investigations of memory. *Neurosci. Biobehav. Rev.* **28**, 497–505 (2004).
35. Lalonde, R. The neurobiological basis of spontaneous alternation. *Neurosci. Biobehav. Rev.* **26**, 91–104 (2002).
36. Cope, E. C. et al. Microglia play an active role in obesity-associated cognitive decline. *J. Neurosci.* **38**, 8889–8904 (2018).
37. Denninger, J. K., Smith, B. M. & Kirby, E. D. Novel object recognition and object location behavioral testing in mice on a budget. *J. Vis. Exp.* **141**, e58593 (2018).
38. Whitehead, J. C. et al. A clinical frailty index in aging mice: comparisons with frailty index data in humans. *J. Gerontol. A Biol. Sci. Med. Sci.* **69**, 621–632 (2014).
39. Hsieh, Y. H. et al. Ultrasonication-assisted synthesis of alcohol-based deep eutectic solvents for extraction of active compounds from ginger. *Ultrason. Sonochem.* **63**, 104915 (2020).
40. Su, B. et al. A DMS shotgun lipidomics workflow application to facilitate high-throughput, comprehensive lipidomics. *J. Am. Soc. Mass Spectrom.* **32**, 2655–2663 (2021).
41. Jauhiainen, A. et al. Normalization of metabolomics data with applications to correlation maps. *Bioinformatics* **30**, 2155–2161 (2014).
42. Li, B. et al. Performance evaluation and online realization of data-driven normalization methods used in LC/MS based untargeted metabolomics analysis. *Sci. Rep.* **6**, 38881 (2016).
43. Molenaar, M. R. et al. LION/web: a web-based ontology enrichment tool for lipidomic data analysis. *Gigascience* **8**, giz061 (2019).
44. Bolger, A. M., Lohse, M. & Usadel, B. Trimmomatic: a flexible trimmer for Illumina sequence data. *Bioinformatics* **30**, 2114–2120 (2014).
45. Dobin, A. et al. STAR: ultrafast universal RNA-seq aligner. *Bioinformatics* **29**, 15–21 (2013).
46. Liao, Y., Smyth, G. K. & Shi, W. featureCounts: an efficient general purpose program for assigning sequence reads to genomic features. *Bioinformatics* **30**, 923–930 (2014).
47. Leek, J. T. & Storey, J. D. Capturing heterogeneity in gene expression studies by surrogate variable analysis. *PLoS Genet.* **3**, 1724–1735 (2007).

48. Love, M. I., Huber, W. & Anders, S. Moderated estimation of fold change and dispersion for RNA-seq data with DESeq2. *Genome Biol.* **15**, 550 (2014).
49. Coenye, T. Do results obtained with RNA-sequencing require independent verification? *Biofilm* **3**, 100043 (2021).
50. Hughes, T. R. Validation' in genome-scale research. *J. Biol.* **8**, 3 (2009).
51. Panina, Y., Germond, A., Masui, S. & Watanabe, T. M. Validation of common housekeeping genes as reference for qPCR gene expression analysis during iPS Reprogramming process. *Sci. Rep.* **8**, 8716 (2018).
52. Singh, P. P. & Benayoun, B. A. Considerations for reproducible omics in aging research. *Nat. Aging* **3**, 921–930 (2023).
53. Chen, Y. & Meltzer, P. S. Gene expression analysis via multidimensional scaling. *Curr. Protoc. Bioinforma.* **7**, 7.11 (2005).
54. Yu, G., Wang, L. G., Han, Y. & He, Q. Y. clusterProfiler: an R package for comparing biological themes among gene clusters. *Omics* **16**, 284–287 (2012).
55. Thorwald, M. A., Silva, J., Head, E. & Finch, C. E. Amyloid futures in the expanding pathology of brain aging and dementia. *Alzheimers Dement* **19**, 2605–2617 (2023).
56. Debarba, L. K., Jayarathne, H. S. M., Miller, R. A., Garratt, M. & Sadagurski, M. 17- α -Estradiol Has Sex-Specific Effects on Neuroinflammation That Are Partly Reversed by Gonadectomy. *J. Gerontol. A Biol. Sci. Med. Sci.* **77**, 66–74 (2022).
57. Sadagurski, M., Cady, G. & Miller, R. A. Anti-aging drugs reduce hypothalamic inflammation in a sex-specific manner. *Aging Cell* **16**, 652–660 (2017).
58. Pabis, K. et al. The impact of short-lived controls on the interpretation of lifespan experiments and progress in geroscience - Through the lens of the 900-day rule. *Ageing Res. Rev.* **101**, 102512 (2024).
59. Montagne, A. et al. APOE4 accelerates advanced-stage vascular and neurodegenerative disorder in old Alzheimer's mice via cyclophilin A independently of amyloid- β . *Nat. Aging* **1**, 506–520 (2021).
60. Horvath, S. DNA methylation age of human tissues and cell types. *Genome Biol.* **14**, R115 (2013).
61. Liu, Y. et al. Plasma lipidome is dysregulated in Alzheimer's disease and is associated with disease risk genes. *Transl. Psychiatry* **11**, 344 (2021).
62. Wang, T. et al. APOE ϵ 2 resilience for Alzheimer's disease is mediated by plasma lipid species: Analysis of three independent cohort studies. *Alzheimers Dement* **18**, 2151–2166 (2022).
63. Cutler, R. G. et al. Involvement of oxidative stress-induced abnormalities in ceramide and cholesterol metabolism in brain aging and Alzheimer's disease. *Proc. Natl Acad. Sci. USA* **101**, 2070–2075 (2004).
64. Pradas, I. et al. Long-lived Humans Have a Unique Plasma Sphingolipidome. *J. Gerontol. A Biol. Sci. Med. Sci.* **77**, 728–735 (2022).
65. Miranda, A. M. et al. Effects of APOE4 allelic dosage on lipidomic signatures in the entorhinal cortex of aged mice. *Transl. Psychiatry* **12**, 129 (2022).
66. Bandaru, V. V. et al. ApoE4 disrupts sterol and sphingolipid metabolism in Alzheimer's but not normal brain. *Neurobiol. Aging* **30**, 591–599 (2009).
67. Kosicek, M. & Hecimovic, S. Phospholipids and Alzheimer's disease: alterations, mechanisms and potential biomarkers. *Int. J. Mol. Sci.* **14**, 1310–1322 (2013).
68. Zhu, L. et al. Phospholipid dysregulation contributes to ApoE4-associated cognitive deficits in Alzheimer's disease pathogenesis. *Proc. Natl Acad. Sci. USA* **112**, 11965–11970 (2015).
69. Lefterov, I. et al. APOE2 orchestrated differences in transcriptomic and lipidomic profiles of postmortem AD brain. *Alzheimers Res. Ther.* **11**, 113 (2019).
70. Brown, C. M., Choi, E., Xu, Q., Vitek, M. P. & Colton, C. A. The APOE4 genotype alters the response of microglia and macrophages to 17 β -estradiol. *Neurobiol. Aging* **29**, 1783–1794 (2008).
71. Gale, S. C. et al. APOE4 is associated with enhanced in vivo innate immune responses in human subjects. *J. Allergy Clin. Immunol.* **134**, 127–134 (2014).
72. Vitek, M. P., Brown, C. M. & Colton, C. A. APOE genotype-specific differences in the innate immune response. *Neurobiol. Aging* **30**, 1350–1360 (2009).
73. Morimoto, M. et al. Haptoglobin Regulates Macrophage/Microglia-Induced Inflammation and Prevents Ischemic Brain Damage Via Binding to HMGB1. *J. Am. Heart Assoc.* **11**, e024424 (2022).
74. Singh, P. et al. Taurine deficiency as a driver of aging. *Science* **380**, eabn9257 (2023).
75. Rodriguez, G. A., Burns, M. P., Weeber, E. J. & Rebeck, G. W. Young APOE4 targeted replacement mice exhibit poor spatial learning and memory, with reduced dendritic spine density in the medial entorhinal cortex. *Learn Mem.* **20**, 256–266 (2013).
76. van Heuvelen, M. J. G., van der Lei, M. B., Alferink, P. M., Roemers, P. & van der Zee, E. A. Cognitive deficits in human ApoE4 knock-in mice: A systematic review and meta-analysis. *Behav. Brain Res.* **471**, 115123 (2024).
77. Di Battista, A. M., Heinsinger, N. M. & Rebeck, G. W. Alzheimer's Disease Genetic Risk Factor APOE- ϵ 4 Also Affects Normal Brain Function. *Curr. Alzheimer Res.* **13**, 1200–1207 (2016).
78. Chen, Y., Durakoglugil, M. S., Xian, X. & Herz, J. ApoE4 reduces glutamate receptor function and synaptic plasticity by selectively impairing ApoE receptor recycling. *Proc. Natl Acad. Sci. USA* **107**, 12011–12016 (2010).
79. Stephen, T. L., Brenningstall, B., Suresh, S., McGill, C. J. & Pike, C. J. APOE genotype and biological sex regulate astroglial interactions with amyloid plaques in Alzheimer's disease mice. *J. Neuroinflammation* **19**, 286 (2022).
80. Stephen, T. L. et al. APOE genotype and sex affect microglial interactions with plaques in Alzheimer's disease mice. *Acta Neuropathol. Commun.* **7**, 82 (2019).
81. Trommer, B. L. et al. ApoE isoform affects LTP in human targeted replacement mice. *Neuroreport* **15**, 2655–2658 (2004).
82. Garrido, A., De La Serna, M., De La Fuente, M., Marco, E. M. & López-Gallardo, M. Neuronal and glial region dependent changes in female mice from a model of premature aging. *Exp. Gerontol.* **146**, 111224 (2021).
83. Grimaldi, A. et al. Neuroinflammatory processes, A1 Astrocyte activation and protein aggregation in the retina of Alzheimer's disease patients, possible biomarkers for early diagnosis. *Front Neurosci.* **13**, 925 (2019).
84. Zhang, H. & Forman, H. J. 4-hydroxynonenal-mediated signaling and aging. *Free Radic. Biol. Med.* **111**, 219–225 (2017).
85. Kao, Y. C., Ho, P. C., Tu, Y. K., Jou, I. M. & Tsai, K. J. Lipids and Alzheimer's Disease. *Int. J. Mol. Sci.* **21**, 1505 (2020).
86. Panov, A. V. & Dikalov, S. I. Cardiolipin, Perhydroxyl radicals, and lipid peroxidation in mitochondrial dysfunctions and aging. *Oxid. Med Cell Longev.* **2020**, 1323028 (2020).
87. Thorwald, M. A. et al. Iron-associated lipid peroxidation in Alzheimer's disease is increased in lipid rafts with decreased ferroptosis suppressors, tested by chelation in mice. *Alzheimers Dement.* **21**, e14541 (2025).
88. Taxier, L. R. et al. APOE4 homozygote females are resistant to the beneficial effects of 17 β -estradiol on memory and CA1 dendritic spine density in the EFAD mouse model of Alzheimer's disease. *Neurobiol. Aging* **118**, 13–24 (2022).
89. Peters, R. Ageing and the brain. *Postgrad. Med. J.* **82**, 84–88 (2006).
90. Volpi, E., Nazemi, R. & Fujita, S. Muscle tissue changes with aging. *Curr. Opin. Clin. Nutr. Metab. Care* **7**, 405–410 (2004).

91. Anisimova, A. S., Alexandrov, A. I., Makarova, N. E., Gladyshev, V. N. & Dmitriev, S. E. Protein synthesis and quality control in aging. *Aging* **10**, 4269–4288 (2018).
92. Ezkurdia, A., Ramírez, M. J. & Solas, M. Metabolic syndrome as a risk factor for Alzheimer's disease: A Focus on Insulin Resistance. *Int. J. Mol. Sci.* **24** (2023).
93. Xu, M. et al. Apolipoprotein E gene variants and risk of coronary heart disease: a meta-analysis. *Biomed. Res. Int.* **2016**, 3912175 (2016).
94. Dankner, R., Ben Avraham, S., Harats, D. & Chetrit, A. ApoE genotype, lipid profile, exercise, and the associations with cardiovascular morbidity and 18-year mortality. *J. Gerontol. A Biol. Sci. Med. Sci.* **75**, 1887–1893 (2020).
95. Robinson, A. C. et al. Influence of APOE genotype in primary age-related tauopathy. *Acta Neuropathol. Commun.* **8**, 215 (2020).
96. Pirraglia, E., Glodzik, L. & Shao, Y. Lower mortality risk in APOE4 carriers with normal cognitive ageing. *Sci. Rep.* **13**, 15089 (2023).
97. Dücker, C. M. & Brockmöller, J. Genomic variation and pharmacokinetics in old age: a quantitative review of age- vs. genotype-related differences. *Clin. Pharm. Ther.* **105**, 625–640 (2019).
98. 2022 Alzheimer's disease facts and figures. *Alzheimers Dement.* **18**, 700–789 (2022).
99. Hay, M., Barnes, C., Huentelman, M., Brinton, R. & Ryan, L. Hypertension and age-related cognitive impairment: common risk factors and a role for precision aging. *Curr. Hypertens. Rep.* **22**, 80 (2020).
100. Ryan, L. et al. Precision aging: applying precision medicine to the field of cognitive aging. *Front. Aging Neurosci.* **11**, 128 (2019).
101. Riedel, B. C., Thompson, P. M. & Brinton, R. D. Age, APOE and sex: Triad of risk of Alzheimer's disease. *J. Steroid Biochem. Mol. Biol.* **160**, 134–147 (2016).
102. Wang, X., Zhou, W., Ye, T., Lin, X. & Zhang, J. Sex difference in the association of APOE4 with memory decline in mild cognitive impairment. *J. Alzheimers Dis.* **69**, 1161–1169 (2019).
103. Moser, V. A. et al. Microglial transcription profiles in mouse and human are driven by APOE4 and sex. *iScience* **24**, 103238 (2021).
104. Zhao, N. et al. Alzheimer's risk factors age, APOE Genotype, and sex drive distinct molecular pathways. *Neuron* **106**, 727–742.e726 (2020).
105. Green, C. L. et al. Sex and genetic background define the metabolic, physiologic, and molecular response to protein restriction. *Cell Metab.* **34**, 209–226.e205 (2022).
106. Liao, C. Y., Rikke, B. A., Johnson, T. E., Diaz, V. & Nelson, J. F. Genetic variation in the murine lifespan response to dietary restriction: from life extension to life shortening. *Aging Cell* **9**, 92–95 (2010).
107. Christensen, A., McGill, C. J., Qian, W. & Pike, C. J. Effects of obesogenic diet and 17 β -estradiol in female mice with APOE 3/3, 3/4, and 4/4 genotypes. *Front. Aging Neurosci.* **16**, 1415072 (2024).
108. McGill, C. J. et al. Lipidomics Data: Protection against APOE4-associated aging phenotypes with the longevity-promoting intervention 17 α -estradiol in male mice. *FigShare* (2025).
109. McGill, C. J. et al. DNAge methylation data: protection against APOE4-associated aging phenotypes with the longevity-promoting intervention 17 α -estradiol in male mice. *FigShare* (2025).
110. McGill, C. J., Benayoun, B. A. & Pike, C. J. All Code: Protection against APOE4-associated aging phenotypes with the longevity-promoting intervention 17 α -estradiol in male mice. *Github* (2025).

Acknowledgements

This study was supported by a grant from the Cure Alzheimer's Fund (C.J.P., C.E.F., B.A.B.). C.J.M. was supported by NIH/NIA grants T32 AG052374 (S.P. Curran) and F31 AG084279 (C.J.M.). The authors thank the UCLA Lipidomics Laboratory for their contributions and Ms. Tavia Roache, Ms. Bayla Brenningstall and Ms. Tyne McHugh for their experimental contributions. Some images from schematics obtained from Freepik.

Author contributions

C.J.P., B.A.B. and C.E.F. designed the study. C.J.M., A.C., W.Q., M.A.T., J.G.L., S.N. and B.B. performed experiments. C.J.M. performed data analyses. C.J.M. performed bioinformatics analysis, and O.S.W. independently checked the code. C.J.M., B.A.B., and C.J.P. wrote the manuscript. All authors approved the final version of the manuscript.

Competing interests

The authors declare no competing interests.

Additional information

Supplementary information The online version contains supplementary material available at <https://doi.org/10.1038/s43856-025-00942-3>.

Correspondence and requests for materials should be addressed to Bérénice A. Benayoun or Christian J. Pike.

Peer review information *Communications Medicine* thanks the anonymous reviewers for their contribution to the peer review of this work. [A peer review file is available].

Reprints and permissions information is available at <http://www.nature.com/reprints>

Publisher's note Springer Nature remains neutral with regard to jurisdictional claims in published maps and institutional affiliations.

Open Access This article is licensed under a Creative Commons Attribution-NonCommercial-NoDerivatives 4.0 International License, which permits any non-commercial use, sharing, distribution and reproduction in any medium or format, as long as you give appropriate credit to the original author(s) and the source, provide a link to the Creative Commons licence, and indicate if you modified the licensed material. You do not have permission under this licence to share adapted material derived from this article or parts of it. The images or other third party material in this article are included in the article's Creative Commons licence, unless indicated otherwise in a credit line to the material. If material is not included in the article's Creative Commons licence and your intended use is not permitted by statutory regulation or exceeds the permitted use, you will need to obtain permission directly from the copyright holder. To view a copy of this licence, visit <http://creativecommons.org/licenses/by-nc-nd/4.0/>.

© The Author(s) 2025